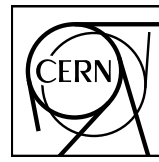


EUROPEAN ORGANIZATION FOR NUCLEAR RESEARCH



CERN-EP-2023-134
12 July 2023

Pseudorapidity dependence of anisotropic flow and its decorrelations using long-range multiparticle correlations in Pb–Pb and Xe–Xe collisions

ALICE Collaboration*

Abstract

The pseudorapidity dependence of elliptic (v_2), triangular (v_3), and quadrangular (v_4) flow coefficients of charged particles measured in Pb–Pb collisions at a centre-of-mass energy per nucleon pair of $\sqrt{s_{\text{NN}}} = 5.02 \text{ TeV}$ and in Xe–Xe collisions at $\sqrt{s_{\text{NN}}} = 5.44 \text{ TeV}$ with ALICE at the LHC are presented. The measurements are performed in the pseudorapidity range $-3.5 < \eta < 5$ for various centrality intervals using two- and multi-particle cumulants with the subevent method. The flow probability density function (p.d.f.) is studied with the ratio of flow coefficient v_2 calculated with four- and two-particle cumulant, and suggests that the variance of flow p.d.f. is independent of pseudorapidity. The decorrelation of the flow vector in the longitudinal direction is probed using two-particle correlations. The results measured with respect to different reference regions in pseudorapidity exhibit differences, argued to be a result of saturating decorrelation effect above a certain pseudorapidity separation, in contrast to previous publications which assign this observation to non-flow effects. The results are compared to 3 + 1 dimensional hydrodynamic and the AMPT transport model calculations. Neither of the models is able to simultaneously describe the pseudorapidity dependence of measurements of anisotropic flow and its fluctuations. The results presented in this work highlight shortcomings in our current understanding of initial conditions and subsequent system expansion in the longitudinal direction. Therefore, they provide input for its improvement.

© 2023 CERN for the benefit of the ALICE Collaboration.

Reproduction of this article or parts of it is allowed as specified in the CC-BY-4.0 license.

*See Appendix A for the list of collaboration members

1 Introduction

There is significant evidence for the production of strongly coupled plasma of quarks and gluons (QGP) in ultra relativistic heavy-ion collisions, as measured by RHIC and LHC experiments [1–5]. Several probes are used to determine the properties of this medium, with measurements of anisotropic flow being among the most powerful ones [6]. The nuclear overlap region of two colliding nuclei forms an initial spatial anisotropy, which is transformed, during the expansion of the subsequently created medium, into an anisotropic azimuthal particle distribution. This anisotropy is quantified based on the Fourier transform of the azimuthal particle distribution [7]

$$\frac{dN}{d\varphi} \propto f(\varphi) = \frac{1}{2\pi} \left[1 + 2 \sum_{n=1}^{\infty} v_n \cos(n[\varphi - \Psi_n]) \right] ,$$

where φ is the azimuthal angle of the emitted particles, Ψ_n is the n^{th} order flow symmetry plane and $v_n = \langle \cos(n[\varphi - \Psi_n]) \rangle$ the n^{th} anisotropic flow coefficient. Here, $\langle \dots \rangle$ denotes an average over all particles in a single event. Together the v_n and Ψ_n define the n^{th} order (complex) anisotropic flow $V_n \equiv v_n e^{in\Psi_n}$, with $v_n = |V_n|$ representing the magnitude of V_n and Ψ_n its angle.

Anisotropic flow characterises the degree of collective motion of produced particles relative to the symmetry plane vector of a heavy-ion collision. It arises as a direct response to the initial geometry of the overlapping region of colliding nuclei, expressed in terms of eccentricity ε_n for $n \leq 4$ [8, 9]. The most pronounced component is the elliptic flow, V_2 , related to the collision ellipticity that reflects the almond shape of the nucleus overlap, while higher order harmonics appear as a result of event-by-event fluctuations of the initial transverse density profiles. Anisotropic flow measurements have been studied in great detail both experimentally and theoretically, thereby allowing the determination of crucial information on the initial conditions and the transport properties of the QGP [10–13], such as the shear viscosity over entropy density ratio, η/s , which was found to be near to the universal lower bound of $1/4\pi$ [14]. In these studies, anisotropic flow was usually assumed to be driven by a boost invariant initial spatial anisotropy, and experimental measurements were interpreted as anisotropy with respect to an event-averaged symmetry plane.

This assumption has been challenged by several measurements of the pseudorapidity (η) dependence of anisotropic flow that revealed longitudinal fluctuations of the flow vectors V_n [15–18]. This can be interpreted as decorrelation of the flow magnitudes and/or symmetry plane angles between two different η windows. Measurements exploiting multiparticle correlations suggest that fluctuations in both the flow magnitude and the symmetry plane contribute equally to the flow vector decorrelation [17]. It was argued in Ref. [19] that these effects are connected to the fluctuating initial state, where the transverse shape of the initially produced system fluctuates not only on an event-by-event basis, but also within an event, and it depends on η . Indeed, many theoretical studies based on hydrodynamic [20–22] and transport models [19, 23] showed that the decorrelations are connected to the longitudinal fluctuations in the initial state, with a possible additional contribution from early time hydrodynamic fluctuations [24], but only weak dependence on the η/s of the QGP [21, 24]. Measurements of anisotropic flow and its fluctuations as a function of pseudorapidity, therefore, represent an important ingredient to constrain the three-dimensional initial conditions and the QGP expansion in longitudinal direction [25–27].

It was found that comparison between measurements from Pb–Pb and Xe–Xe collisions offers a unique possibility to test the hydrodynamic framework under variations of the nuclear mass number and geometry of the collisions [28–30]. Recent results on longitudinal flow fluctuations in both Pb–Pb and Xe–Xe collisions showed that the hydrodynamic models that successfully describe the transverse dynamics of the medium evolution, do not reproduce the longitudinal structure of the initial state [18]. Thus, studying results from collision systems of different sizes can bring additional insight into our understanding of the properties of the QGP.

This letter presents measurements of the pseudorapidity dependence of anisotropic flow coefficients v_2 , v_3 and v_4 in Pb–Pb collisions at collision energy $\sqrt{s_{\text{NN}}} = 5.02 \text{ TeV}$ and Xe–Xe collisions at $\sqrt{s_{\text{NN}}} = 5.44 \text{ TeV}$ within a wide pseudorapidity range, $-3.5 < \eta < 5.0$, with the ALICE detector. The measurements are based on two- and four-particle cumulants, $v_n\{2\}$ and $v_n\{4\}$, respectively [31, 32]. To suppress contamination from short-range correlations, denoted as non-flow, particles are measured in different subevents widely separated in phase space by imposing a pseudorapidity gap, $|\Delta\eta|$, between them. The large detector acceptance, together with the state-of-the-art measurement techniques, enables us to perform these studies in a wider pseudorapidity range and with a larger pseudorapidity separation of $|\Delta\eta| > 3.8$ compared to previous measurements done at the LHC [16, 17, 33]. The results presented in this letter improve previous ALICE measurements [34] by significantly reducing the systematic uncertainties dominated by those stemming from corrections for secondary particles and non-flow contamination. In addition, the longitudinal flow vector fluctuations are investigated using the ratio of two-particle correlators calculated in subevents at different pseudorapidities. Both centrality and pseudorapidity dependences are discussed. The results are compared with calculations from a 3 + 1 dimensional CLVisc hydrodynamic model [35] and the AMPT transport model [36].

2 Observable definitions

Anisotropic flow and its fluctuations are measured with two- and four-particle cumulants, and a decorrelation ratio, respectively, with the use of m -particle azimuthal correlations. The m -particle azimuthal correlations are calculated with the generic framework [32], which is an effective way to obtain correlation of any order corrected for detector effects.

Differential observables, such as those presented in this work, are measured by correlating the so-called particles of interest, POI, in the desired narrow pseudorapidity interval with respect to reference particles, RFP, measured in a wide pseudorapidity range. If the η intervals of POI and RFP are close to each other, such correlations are affected by non-flow contamination, that mainly arise from correlations among the jet constituents. These are suppressed by imposing a pseudorapidity gap, $|\Delta\eta|$, between regions called subevents. In this analysis, correlations are calculated in specific regions in η , which can naturally be considered as subevents. The choice of these subevents allows us to perform longitudinal flow measurements while suppressing the contribution from non-flow.

The regions used for the measurements presented in this article are schematically illustrated in Figs. 1 and 2. Regions A and D correspond to very forward pseudorapidities, while regions B and C are on either side of the symmetry line $\eta = 0$.

Within a traditional approach, flow coefficients differential in pseudorapidity are obtained from two-particle cumulants as

$$v_n^X\{2\} = \frac{\langle\langle 2' \rangle\rangle}{\sqrt{\langle\langle 2 \rangle\rangle}} = \frac{\langle v_n^X v_n^Y \rangle}{\sqrt{\langle v_n^X v_n^Y \rangle}}, \quad (1)$$

where the v_n and v'_n are the reference and differential flow, respectively, and X, Y stand for different reference regions for particle correlations in pseudorapidity. The single angular brackets $\langle \cdot \rangle$ represent an average over events with similar centrality, and the double angular brackets $\langle\langle \cdot \rangle\rangle$ an average over particles within an event, and over events. It is further assumed that the reference flow is symmetric, $v_n^X = v_n^Y$, as warranted for symmetric collision systems such as Pb–Pb and Xe–Xe, presented in this work. The $\langle\langle m \rangle\rangle$ denotes the m -particle correlation, in particular the $\langle\langle 2 \rangle\rangle$ represents correlations between two RFP, and $\langle\langle 2' \rangle\rangle$ correlation between RFP and POI. These correlations are defined as:

$$\begin{aligned} \langle\langle 2 \rangle\rangle &= \langle\langle \cos[n(\phi_1^X - \phi_2^Y)] \rangle\rangle, \\ \langle\langle 2' \rangle\rangle &= \langle\langle \cos[n(\phi_1^X - \phi_2^Y)] \rangle\rangle, \end{aligned} \quad (2)$$

with $\varphi_k^{X,Y}$ representing the azimuthal angle of RFP from reference regions X or Y , and $\varphi_k'^X$ representing the azimuthal angle of POI in a given narrow interval in η .

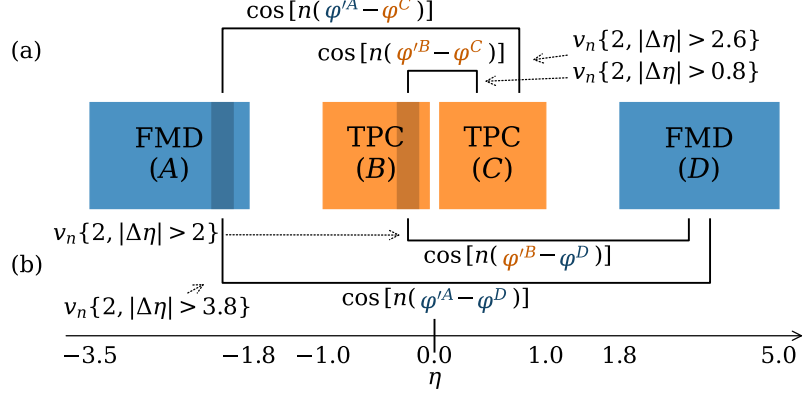


Figure 1: Illustration of correlator methods showing calculation of $v_n\{2\}$ using either a small (a) or large (b) separation in pseudorapidity. Darker bands indicate where the differential measurement is performed (i.e. particles of interest) while the other end of the connecting lines indicate reference particles.

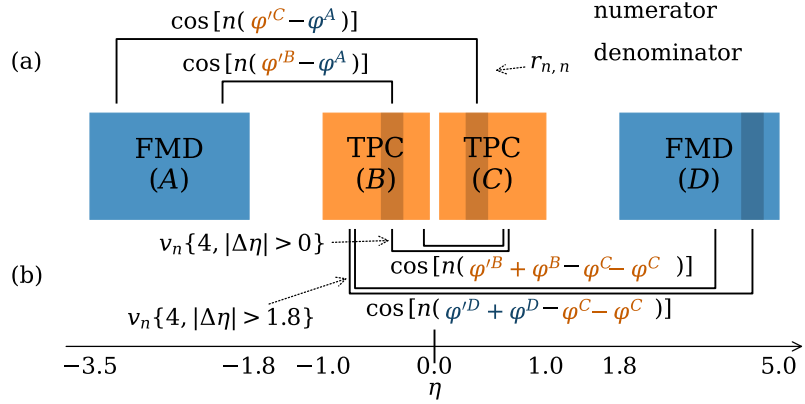


Figure 2: Illustration of correlator methods showing calculation of the decorrelation effect (a) as well as $v_n\{4\}$ (b). Darker bands indicate where the differential measurement is performed (i.e. particles of interest) while the other end of the connecting lines indicate reference particles.

The analysis is carried out with two choices of reference region, as illustrated in Fig. 1. In the first case, the reference region is chosen from midrapidity, i.e. either region B or C . In this configuration, the RFP are correlated with POI in region C or D , or B or A , respectively. That is, RFP at negative (positive) midrapidity are correlated with POI at positive (negative) mid or forward rapidity. In such configurations where the correlated particles are taken from neighbouring regions, it is important to suppress non-flow by avoiding correlations near the edge of the regions, i.e. when the difference between POI and RFP is $|\Delta\eta| \approx 0$. Therefore, only a specific η range in the corresponding reference region is chosen, in particular $0.8 < |\eta| < 1.0$. This choice effectively results in an η -gap for midrapidity measurements of $|\Delta\eta| > 0.8$, while forward measurements have a larger separation of $|\Delta\eta| > 2.6$.

The case where the reference region is positioned in C is illustrated in Fig. 1(a).

In the second case, the reference region is chosen to be at forward rapidity. In this configuration, there are again several options to correlate the RFP with POI. The particles taken from reference regions A (or D), can be correlated with POI from C or D (or A or B). In this way, the pseudorapidity separation between RFP and POI is increased to $|\Delta\eta| > 2.0$ and $|\Delta\eta| > 3.8$ for mid- and forward rapidity measurements,

respectively. Therefore, this configuration excludes more short-range correlations arising from non-flow as compared to the first case. This configuration, in particular the case where the reference region is chosen to be D , is illustrated in Fig. 1(b).

The advantage of measuring flow coefficients via m -particle cumulants for $m > 2$ is the suppression of lower order non-flow correlations by definition [31], including those that stem from non-flow effects. To further suppress remaining non-flow originating in multiparticle short-range correlations, the subevent method was recently introduced to higher order cumulants, too [37, 38]. The differential flow is determined using the four-particle cumulant defined as

$$v_n'^X \{4\} = -\frac{\langle\langle 4' \rangle\rangle - 2 \cdot \langle\langle 2' \rangle\rangle \langle\langle 2 \rangle\rangle}{(-\langle\langle 4 \rangle\rangle - 2 \cdot \langle\langle 2 \rangle\rangle^2)^{3/4}} = \frac{\langle v_n'^X v_n^3 \rangle}{\langle v_n^4 \rangle^{3/4}}, \quad (3)$$

where the two-particle correlations are calculated in the same way as in Eq. (2). Four-particle correlations are obtained as

$$\begin{aligned} \langle\langle 4 \rangle\rangle &= \langle\langle \cos[n(\varphi_1^X + \varphi_2^X - \varphi_3^Y - \varphi_4^Y)] \rangle\rangle, \\ \langle\langle 4' \rangle\rangle &= \langle\langle \cos[n(\varphi_1'^X + \varphi_2^X - \varphi_3^Y - \varphi_4^Y)] \rangle\rangle. \end{aligned} \quad (4)$$

The choice of the subevents for the $v_n \{4\}$ measurements is the same as in the case of the two-particle cumulant measurement discussed above and as illustrated in Fig. 2(b). Reference regions only at midrapidity, B or C , are used for this measurement. As this observable is less influenced by non-flow, it is possible to exploit the whole η range of the reference region to minimise statistical uncertainties, yielding an η -gap of $|\Delta\eta| > 0$ for midrapidity measurements, and $|\Delta\eta| > 2.0$ for forward measurements.

In order to investigate the longitudinal fluctuations of the flow vector, a decorrelation ratio $r_{n|n}$ [16] is used. As illustrated in Fig. 2(a), it is formed as the ratio of the opposite-side two-particle correlation between the reference region and the region of interest (i.e. RFP from region A (D) correlated with POI in narrow η intervals from region C (B)) to the same-side correlation (i.e. RFP from region A (D) correlated with POI in narrow η intervals from region B (C)),

$$r_{n|n} = \frac{\langle \cos[n(\varphi_1'^{-X} - \varphi_2^Y)] \rangle}{\langle \cos[n(\varphi_1'^X - \varphi_2^Y)] \rangle} = \frac{\langle v_n'^{-X} v_n^Y \cos[n(\Psi_n'^{-X} - \Psi_n^Y)] \rangle}{\langle v_n'^X v_n^Y \cos[n(\Psi_n'^X - \Psi_n^Y)] \rangle}, \quad (5)$$

where the Ψ_n^Y is the average symmetry plane of a reference region Y , and $\Psi_n'^X$ is the symmetry plane of the given narrow interval in η . Flow vector fluctuations arise from two sources. First, the decorrelation of the symmetry plane, which would manifest in a non-vanishing cosine term, as the symmetry planes Ψ_n at different pseudorapidities would not be equal to each other, or twisted, $\Psi_n'^X \neq \Psi_n^Y$. Second, the decorrelation of the flow magnitude would lead to the product of flow coefficients not being factorised due to additional fluctuation terms dependent on η : $\langle v_n^X v_n^Y \rangle \neq \sqrt{\langle v_n^X \rangle^2} \sqrt{\langle v_n^Y \rangle^2}$. To measure the absolute signal of flow vector fluctuation, the correlations between particles from different η intervals in the numerator of $r_{n|n}$ would be ideally divided with correlations performed between particles from the same η window in the denominator. Such configuration would, however, introduce significant non-flow background, as the main characteristic of these correlations is the proximity of particles in η . Therefore, the $r_{n|n}$ observable defined in Eq. (5) is used, which quantifies the relative flow fluctuations between η and $-\eta$. It ensures that POI have the same absolute pseudorapidity ($\eta = \eta^C = -\eta^B$). If neither v_n nor Ψ_n fluctuate along the longitudinal direction, then $r_{n|n}$ is expected to converge to unity. If either of these effects, or both, are present, then the numerator of $r_{n|n}$ is smaller than the denominator, and hence $r_{n|n}$ will deviate from unity, with deviations growing stronger with increasing η (i.e. larger relative pseudorapidity difference). However, remaining short-range non-flow effects may also give rise to a fake decorrelation signal, as they would increase the value of the denominator.

3 Experimental Setup

A detailed description of the ALICE apparatus can be found in Ref. [39, 40]. The relevant detectors for the presented results are the Inner Tracking System (ITS) [41], a silicon detector consisting of 6 cylindrical layers close to the collision point; the Time Projection Chamber (TPC) [42], which is the main tracking detector in ALICE; and the Forward Multiplicity Detector (FMD) [43], a silicon strip detector which measures the multiplicity of charged particles at forward rapidities. Finally, the V0 scintillator arrays are used for online event selection and offline centrality determination. These two arrays are placed at very forward rapidities and provide high-resolution timing and approximate sum multiplicity measurements offline [44].

Charged-particle trajectories measured by both ITS and TPC combined are limited to $|\eta| < 0.9$. However, tracks measured with the TPC only, that is, without matching tracks to other hit-producing devices, can be extended to $|\eta| < 1.5$, with a slightly reduced transverse momentum resolution. Particle trajectories are reconstructed in $0.2 < p_T < 5 \text{ GeV}/c$, with the requirement of at least one space point in the two inner most layers of the ITS, at least 70 (out of 159) space points in the TPC, and a largest transverse and longitudinal distance (DCA) to the primary vertex of 0.0182 cm and 2 cm, respectively. The upper cut-off on transverse momentum is imposed to limit the contribution from high- p_T particles mostly from jets and to ensure relatively uniform tracking efficiency. The limit on pseudorapidity is imposed to ensure full TPC coverage. Tracking efficiencies and detector acceptance effects are corrected for using per-particle weights (for details see Ref. [32]). The flow measurements in the central region of pseudorapidity are extrapolated to $p_T = 0$, based on simulations with AMPT model calculations as input, to make the measurements comparable to those at forward pseudorapidity. The correction was obtained as the ratio of v_n with no p_T cut to v_n with the cut used for the analysis. Only primary particles were used to remove any detector effects in the calculations.

The FMD covers $-3.5 < \eta < -1.8$ and $1.8 < \eta < 5$ with high resolution in pseudorapidity and 20 segments in azimuth. Due to various technical and engineering considerations, the direct line-of-sight from the FMD sub-detectors to the collision point is obscured by relatively large amounts of material which require careful study of secondary particle production and associated corrections [45]. The FMD does not provide any tracking capabilities on its own and can therefore not distinguish between primary particles [46] and particles produced in decays or surrounding material. Instead, the effect of secondary particles on the observed azimuthal particle distribution was studied, with emphasis on the relative deflection of secondary particles with respect to the primary particle ($\delta\phi$). The Fourier transform \mathcal{F} of the resulting $dN/d(\delta\phi)$ distribution then corrects for the deflection of secondary particles relative to their primary origin, so that the differential flow measurement becomes $\langle\langle v'_n v_n \rangle\rangle^{\text{primary}} = \mathcal{F}^{-1} \langle\langle v'_n v_n \rangle\rangle^{\text{inclusive}}$, where *inclusive* means the measured correlation of both primary *and* secondary particles. The transformation \mathcal{F} (a factor in Fourier space) depends on the material traversed by the particles and, as such, is dependent on the pseudorapidity of the particles and on the position of the interaction point in the beam direction z . The first order effect of the material is to amplify the primary signal proportionally, and no significant dependence of \mathcal{F} on collision centrality is found. The resulting correction for the effect of secondary particles ranges from 1.1 to 1.6, depending on the pseudorapidity, primary vertex z coordinate, and the order of the flow harmonic. Detector acceptances are corrected for using per-azimuth-segment weights.

The results presented in this letter are based on data acquired during LHC Run 2 in 2015 for Pb–Pb collisions at $\sqrt{s_{\text{NN}}} = 5.02 \text{ TeV}$ and in 2017 for Xe–Xe at $\sqrt{s_{\text{NN}}} = 5.44 \text{ TeV}$. The event selection involves a centrality estimate based on the amplitudes of the signals in both arrays of the V0 detectors [47], and a constraint on events within 10 cm from the primary vertex. Selection criteria on the correlation between the forward detectors V0 and FMD as well as a veto on multi-vertex events are applied to select beam-crossings and reject pileup as well as outlier events. In total, 10^7 and 10^6 collisions of Pb–Pb and Xe–Xe, respectively, were analysed.

4 Systematic uncertainties

The systematic uncertainties stemming from event selection, multi-vertex veto, and outlier rejection are investigated by tightening and relaxing the selection criteria used in this analysis, and the effects are found to be negligible. Variations in the accepted primary vertex z coordinate influence the acceptance of the detectors. This contribution accounts for at most 1% uncertainty in the most peripheral collisions. The systematic uncertainty associated with estimating collision centrality is studied by defining centrality intervals using the multiplicity distribution measured at midrapidity [48] rather than in the V0 amplitude. The uncertainty is found to be at most 1% in midcentral collisions and negligible in the most peripheral and central collisions.

The effects of the track selection at midrapidity are explored by performing an independent analysis with varied values of the selection criteria, and is summarised in the following. Increasing the number of required TPC space points was found to be negligible. Variations in the required DCA of tracks in both transverse and longitudinal direction to provide different sensitivity to contamination from secondary tracks result in a 1 to 3% systematic uncertainty, larger for most central collisions and $v_n\{4\}$ results. *Hybrid tracks*, which combine information from three different types of tracks in order to achieve uniform azimuthal acceptance and the best transverse momentum resolution, are used for systematic variation of the track reconstruction procedure. A 1 to 6% systematic uncertainty is found, smallest for v_2 , and largest for the highest harmonic, v_4 . The uncertainty arising from the extrapolation of midrapidity v_n to $p_T = 0$ was estimated by varying the maximum value of the p_T selection, and was found to be 1%.

Systematic uncertainties originating from secondary particle production on a material in front of the FMD are investigated by varying the material density by $\pm 10\%$ using Monte Carlo simulations. The resulting systematic uncertainty of 2.5% for v_2 , 3% for v_3 , and 3.5% for v_4 , is found. This represents a significant improvement with respect to the previous results [34]. An effective correction for secondary particle production, which compares generator level to post-simulated detector response, to the Fourier space correction (\mathcal{F}), gives a systematic uncertainty ranging from 1% for v_2 to 4% for v_4 . Finally, the systematic uncertainty from generating the secondary correction on simulated rather than experimental data, via detailed analysis of simulated particle trajectories, ranges between 0.5–3%, with values dependent on the order of the harmonic investigated.

As the effects from secondary particles arising from including the FMD detector in the analysis has little or no dependence on centrality nor collision systems, the same corrections for secondary particles in Pb–Pb collisions are applied to the Xe–Xe data, taking into account the smaller overall particle production in these collisions [49].

The weights introduced to account for non-uniform acceptance and efficiencies are in principle dependent on the granularity by which these are determined. The uncertainty related to varying the granularity is investigated and found to be negligible at both mid- and forward rapidity.

The systematic uncertainty of blind regions ('holes') in the FMD is evaluated by comparing the generator level results to full detector response simulations results with interpolation in these holes. This exercise results in 2% systematic uncertainty, applied only in the pseudorapidity regions affected by the acceptance holes of the FMD. Also, the positive and negative pseudorapidity results are compared, as these are expected to be symmetric in symmetric collision systems such as Pb–Pb and Xe–Xe. An uncertainty of at most 2% and 4% at mid- and forward rapidity, respectively, in Pb–Pb collisions, and 2% and 5% in Xe–Xe collisions is assigned, due to the asymmetry introduced into the analysis procedure by corrections for efficiency, acceptance, and secondary particles.

It should be noted that the choice of using two- or multiparticle correlations, with a rapidity gap between POI and RFP to suppress correlations from non-collective behaviour, effectively removes the 2–10% uncertainty that was applied to the previous ALICE results [34].

The different sources listed above were assumed to be uncorrelated and added in quadrature to determine the total systematic uncertainty on the measurement of v_n . These contributions, however, cancel out in the decorrelation ratio $r_{2|2}$, since uncertainties are shared between the numerator and denominator. Therefore, only the statistical uncertainties are reported on this quantity.

5 Results

Figure 3 presents the measurements of $v_2\{2\}$, $v_3\{2\}$ and $v_4\{2\}$ as a function of pseudorapidity and centrality in Pb–Pb collisions at $\sqrt{s_{\text{NN}}} = 5.02$ TeV. The $v_4\{2\}$ measurement at 50–60% collision centrality is not shown due to large statistical uncertainties. The reference region is at midrapidity, and the η -gap between the POI and RFP at mid and forward rapidity is $|\Delta\eta| > 0.8$ and $|\Delta\eta| > 2.6$, respectively (corresponding to the subevent topology illustrated in Fig. 1(a)). The $v_2\{2\}$ measurements show a stronger dependence on collision centrality, while $v_3\{2\}$ and $v_4\{2\}$ reveal only a modest dependence. This is consistent with pseudorapidity integrated measurements [50] explained by v_2 being driven by the average elliptic geometry, while higher order harmonics originate predominantly from its fluctuations.

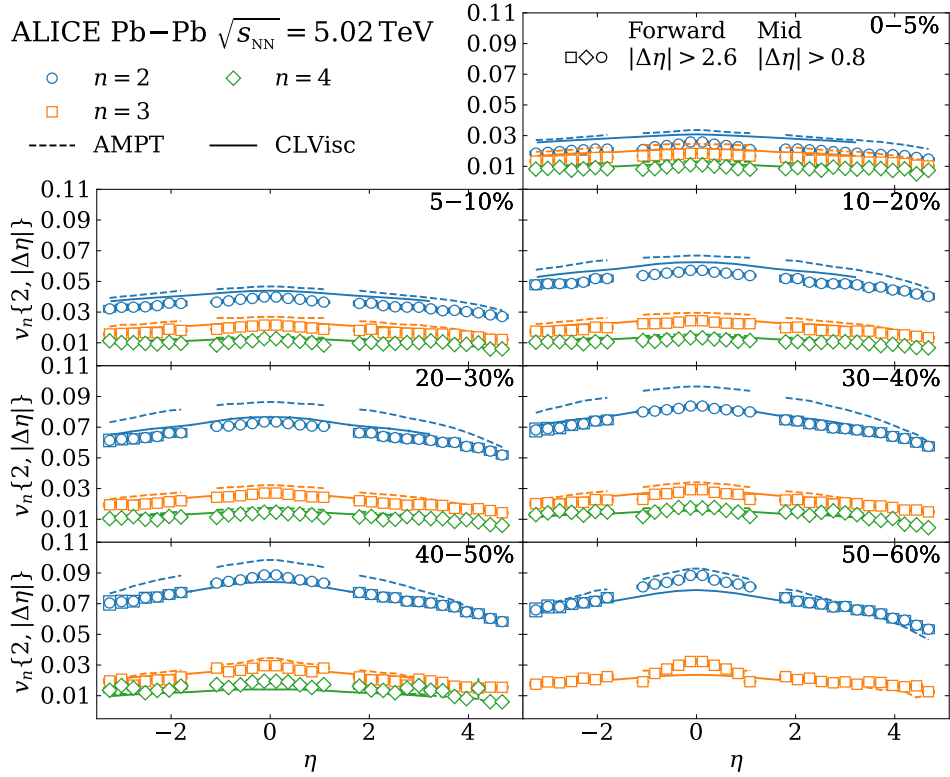


Figure 3: The differential flow measurements, $v_n\{2\}(\eta)$, measured with the 2-particle cumulant and choosing reference particles from the TPC in Pb–Pb collisions at $\sqrt{s_{\text{NN}}} = 5.02$ TeV. The choice of the reference particles results in $|\Delta\eta| > 0.8$ and 2.6 in the mid and forward pseudorapidity regions, respectively. At midrapidity, the results are extrapolated to $p_T = 0$. AMPT and CLVisc model calculations are compared with the results.

Figure 4 shows the pseudorapidity dependence of flow coefficients obtained with large η -gap ($|\Delta\eta| > 2.0$ and $|\Delta\eta| > 3.8$ for mid and forward rapidities, respectively) between POI and RFP choosing forward rapidity for the reference region (corresponding to the subevent topology illustrated in Fig. 1(b)). Also shown are the results of the four-particle cumulant $v_2\{4\}$. A similar trend of $v_n\{m\}$ as a function of centrality and pseudorapidity can be seen as in Fig. 3, except at midrapidity, where the increased η -gap for $v_n\{2\}$, or using higher order cumulant $v_2\{4\}$, leads to almost constant dependence on pseudorapidity compared to the measurements with smaller η -gap reported in Fig. 3.

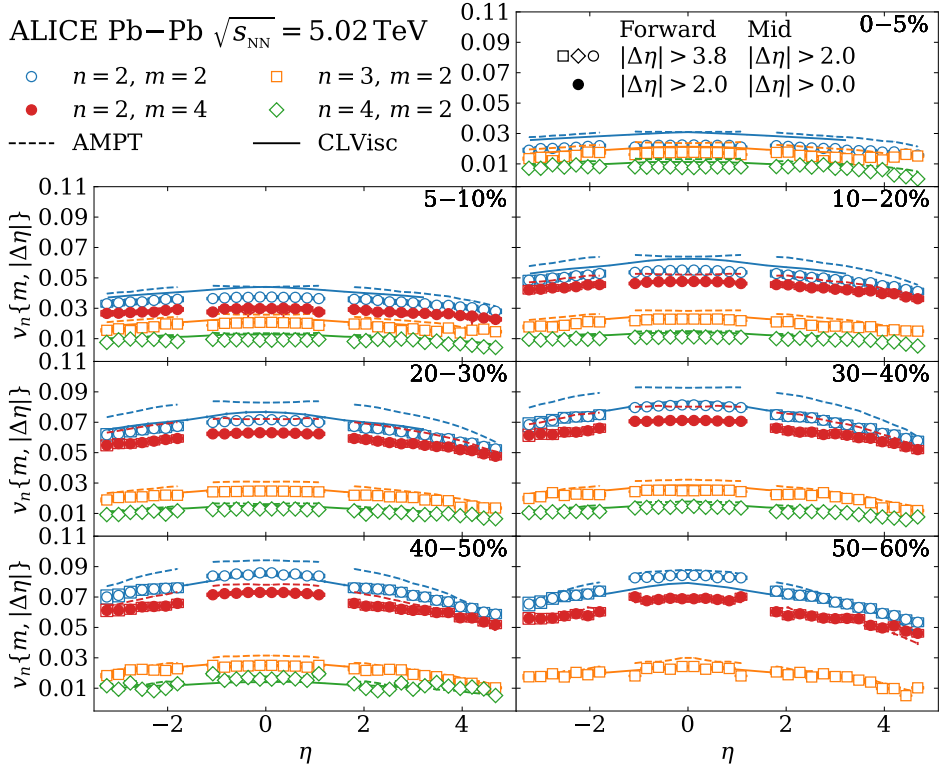


Figure 4: Two-particle cumulant with reference particles chosen from the FMD and 4-particle cumulant with reference particles chosen from the TPC in Pb–Pb collisions at $\sqrt{s_{\text{NN}}} = 5.02 \text{ TeV}$. The pseudorapidity separations are $|\Delta\eta| > 2.0$ and 3.8 for two-particle cumulants for mid and forward rapidities, respectively. For the $v_2\{4\}$ the separations are $|\Delta\eta| > 0$ and 2.0 for mid and forward rapidities, respectively. At mid rapidity, the results are extrapolated to $p_T = 0$. AMPT and CLVisc model calculations are compared with the results.

To better appreciate the difference between the results shown in Figs. 3 and 4, Fig. 5 presents the ratio of $v_n\{2\}$ with reference region at midrapidity, and the $v_2\{4\}$ results, to the $v_n\{2\}$ results using the forward reference region. The relevant ratio for $v_4\{2\}$ has large statistical uncertainties and is therefore not shown. The fluctuation of data points at large pseudorapidity, in particular for larger centralities, are remnants of systematic effects which have not been identified and therefore not quantified, and are further accentuated when calculating the ratio. The ratio exhibits no significant dependence on the pseudorapidity, except near $\eta = 0$. This qualitative difference only at midrapidity could be understood as a result of better suppression of short-range correlations, or non-flow, when a larger η -gap is used. At forward pseudorapidity, where the η -gap is large, the contribution from such correlations may be already sufficiently suppressed, as the data suggest.

The clear difference between the values of v_2 using two- and four-particle cumulants, reflected by their ratio being significantly smaller than unity, can be mainly attributed to opposite contributions of the event-by-event fluctuations of the flow probability density function, in particular its variance, to different order cumulants [51–54], and partly also to better suppression of non-flow correlations in case of $v_2\{4\}$. The ratio $v_2\{4\}/v_2\{2\}$ is assumed to reflect the ratio $\varepsilon_2\{4\}/\varepsilon_2\{2\}$, since the second order flow magnitude v_2 is proportional to the second order eccentricity ε_2 of the initial overlap region [55–59]. It has previously been reported for the integrated flow measurements that this ratio exhibits a deviation from unity. This deviation is larger in more central collisions, affected by fluctuations in the initial spatial asymmetry [30, 60, 61], and shows potential to constrain the different initial state models. Our measurements of pseudorapidity differential ratio of $v_2\{4\}/v_2\{2\}$, shown in Fig. 5, provide more detailed understanding of flow fluctuations. Similar dependence on centrality as the integrated measurements [60] is reported, but the results indicate that the variance of v_n , thus also the variance of ε_n in the initial state, is invariant with pseudorapidity. The same observation was reported in Ref. [25] based on hydrodynamic calculations. The authors confirmed that the event-by-event flow fluctuations are only weakly sensitive to pseudorapidity, and are close to the relative eccentricity fluctuations over a wide rapidity range. Therefore, ratios of cumulants of v_n distributions presented here as a function of pseudorapidity provide important input to constraining fluctuations of the 3D initial state [25].

Comparisons with calculations from the AMPT model [62] and hydrodynamic model CLVisc [35] are shown in Figs. 3 and 4 with dashed and full lines, respectively. The AMPT is a hybrid model that evolves fluctuating initial conditions from the HIJING model [63], followed by partonic and hadronic interactions. It gives reasonable descriptions of the rapidity distributions measured in heavy-ion collisions. The CLVisc is a (3 + 1)-dimensional hydrodynamic model that simulates the dynamic evolution of the QGP fireball based on the initial conditions computed with the AMPT model. Because of extra parameters tuning and additional parton smearing in the CLVisc to fit the experimental data, the initial conditions from CLVisc are not identical to those of the AMPT model. The AMPT and CLVisc calculations of the v_n coefficients shown in Fig. 3 and 4 were carried out in a similar way as the analysis of ALICE data presented in this article, using the pseudorapidity ranges and η -gap as illustrated in Fig. 1.

Both AMPT and CLVisc calculations qualitatively follow the trend of the pseudorapidity dependence of v_n found in data. Both models, however, overestimate the v_n coefficients over the whole presented pseudorapidity range in the 30% most central Pb–Pb collisions. In the case of AMPT, that trend continues down to the most peripheral collisions, while CLVisc underestimates the experimental results for the 40–60% collision centrality range. The AMPT calculations with a small η -gap (Fig. 3) show peaked pseudorapidity dependence near $\eta = 0$, while this trend vanishes with large η -gap (Fig. 4), similarly as in data. In contrast, the CLVisc calculations remain unchanged for the two cases. This further substantiates the origin of this peak to be caused by non-flow contributions from short range correlations, since CLVisc produces less of these than the transport AMPT model. Nevertheless, comparison with measurements with forward reference regions (i.e. large η -gap) in Fig. 4 reveals that the CLVisc model predicts a systematically more peaked distribution near midrapidity, while AMPT shows a constant η dependence

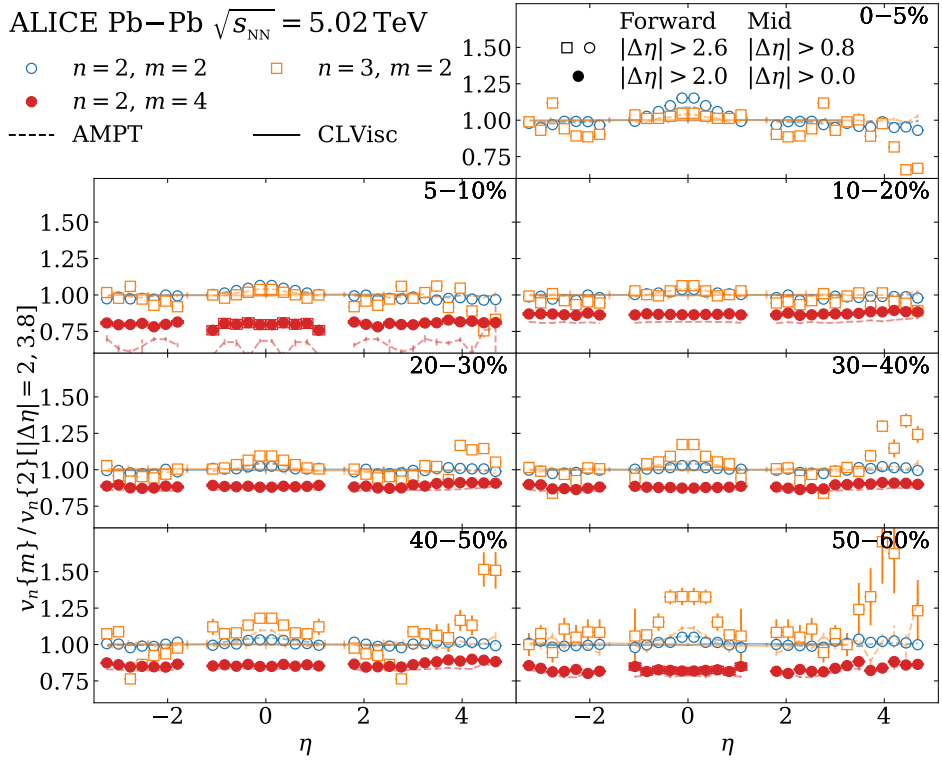


Figure 5: Ratio of two-particle results with a medium-sized pseudorapidity separation and 4-particle results to the two-particle results employing a large pseudorapidity separation between particles of interest and reference particles in Pb–Pb collisions at $\sqrt{s_{\text{NN}}} = 5.02 \text{ TeV}$. Also shown are the same ratios for the AMPT and CLVisc models. For the latter, the ratios are compatible with unity as the CLVisc model produces negligible non-flow [35].

of v_n , which is in qualitative agreement with the data. Other calculations of hydrodynamical models [25, 26, 35] attempted to describe the prior datasets, with no quantitative agreement being reached so far. This suggests, that the longitudinal structure of the initial state or longitudinal evolution of the system are not yet properly understood in these models and more theoretical investigations are warranted.

The flow coefficients $v_n\{2\}$ in Xe–Xe collisions at $\sqrt{s_{\text{NN}}} = 5.44 \text{ TeV}$ are shown as a function of pseudorapidity and centrality in Fig. 6 for the case where the reference region is at midrapidity (i.e. a modest η -gap), and in Fig. 7 when the reference region resides at forward rapidity (i.e. a large η -gap). Due to limited amount of data available from Xe–Xe collisions, the choice of η -gap separation for $v_2\{2\}$ and $v_3\{2\}$ was decreased down to $|\Delta\eta| > 0.4$ at midrapidity and to 2.2 at forward rapidity, and neither the $v_4\{2\}$ nor $v_2\{4\}$ could be measured in these collisions. The results from Xe–Xe collisions show a similar trend as seen in Pb–Pb collisions with roughly 30% larger magnitude in the 5% most central collisions, which was explained by larger deformation of the xenon nucleus [30]. Similarly to Pb–Pb collisions, measurements with RFP from a forward η region lead to a less pronounced dependence on pseudorapidity near midrapidity due to a larger η -gap between the correlated RFP and POI. This is further illustrated in Fig. 8 by the ratio of v_n coefficients obtained with different reference regions, thus different η -gap.

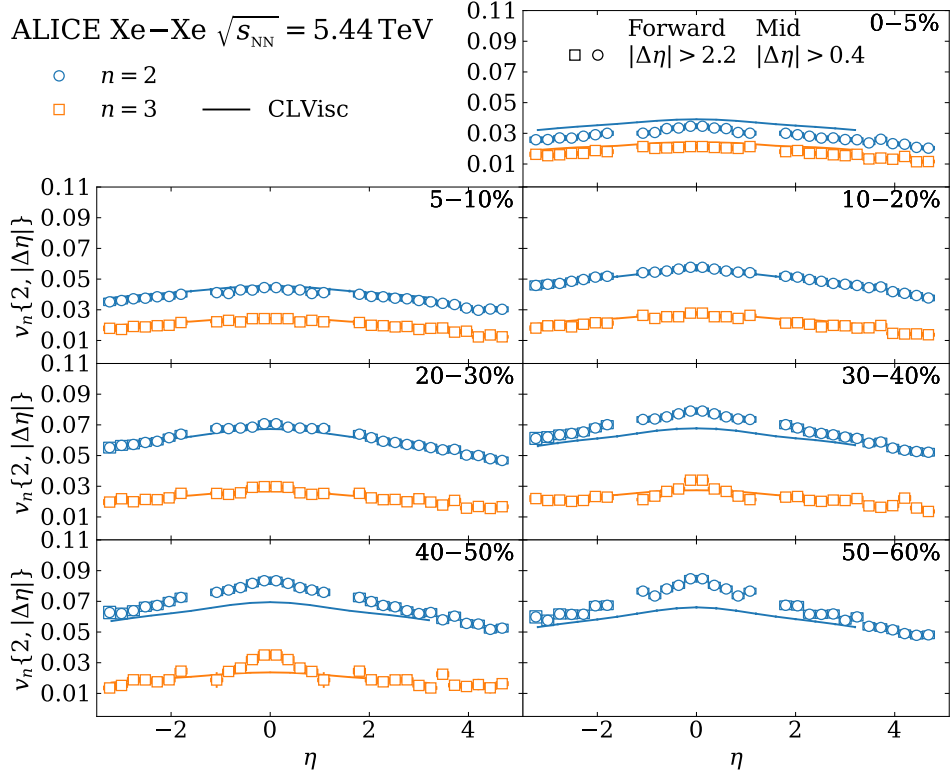


Figure 6: The differential flow measurements, $v_n\{2\}$, measured with the 2-particle cumulant and choosing reference particles from the TPC in Xe–Xe collisions at $\sqrt{s_{\text{NN}}} = 5.44 \text{ TeV}$. The choice of the reference particles results in pseudorapidity separations of $|\Delta\eta| > 0.4$ and 2.2 at mid and forward rapidities, respectively. Also shown are results from the CLVisc model.

Calculations from the CLVisc model [35] are compared with the experimental results in Figs. 6 and 7. The model qualitatively describes the data, although with a more peaked η dependence at midrapidity compared with the results using a large η -gap, and it also overestimates (underestimates) the v_n measurements at central (peripheral) collisions. The shift between the two scenarios happens at higher centrality (around 20%) as compared with the Pb–Pb collisions (around 40%).

Measurements of $r_{2|2}$ as a function of absolute pseudorapidity η for different centrality classes of Pb–Pb collisions at $\sqrt{s_{\text{NN}}} = 5.02 \text{ TeV}$ are presented in Fig. 9. The red and blue markers represent two different

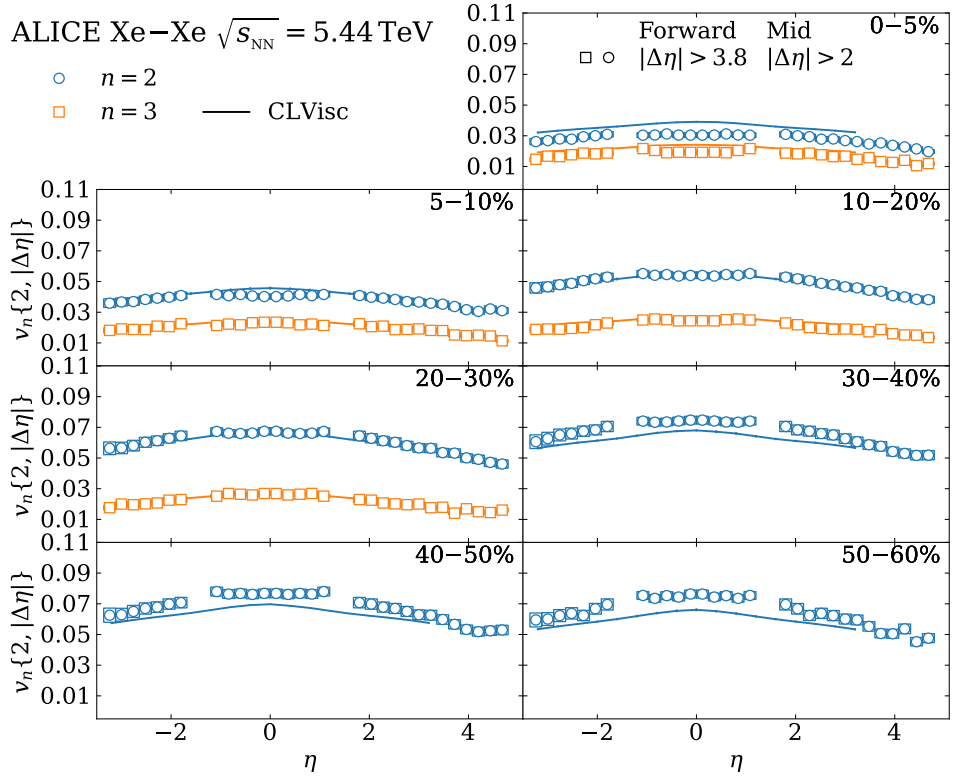


Figure 7: The differential flow measurements, $v_n\{2\}$, measured with the 2-particle cumulant and choosing reference particles chosen from the FMD in Xe–Xe collisions at $\sqrt{s_{\text{NN}}} = 5.02 \text{ TeV}$, with pseudorapidity separations of $|\Delta\eta| > 2.0$ and 3.8 at mid and forward rapidities, respectively. Also shown are results from the CLVisc model.

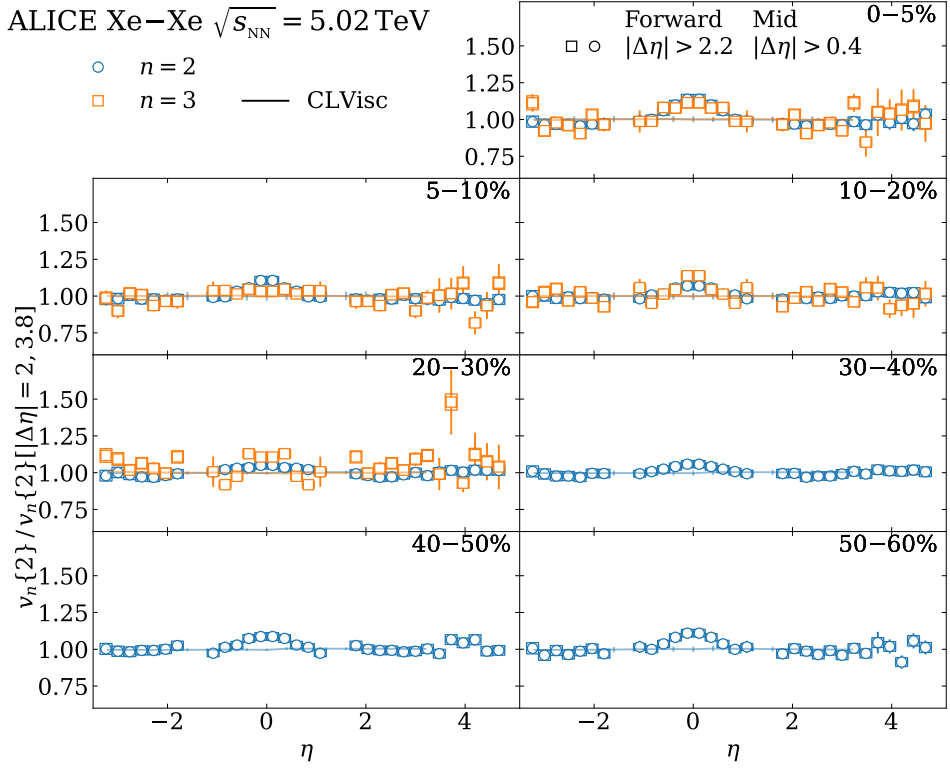


Figure 8: Ratio of two-particle results with a medium-sized separation to the two-particle results employing a large separation between particles of interest and reference particles in Xe–Xe collisions at $\sqrt{s_{\text{NN}}} = 5.44 \text{ TeV}$. Also shown are the same ratios for the AMPT and CLVisc models. For the latter, the ratios are compatible with unity as the CLVisc model produces negligible non-flow [35].

cases of the absolute reference pseudorapidity regions, chosen to be $2 < \eta_{\text{ref}} < 2.4$ or $2.8 < \eta_{\text{ref}} < 3.2$, respectively (Fig. 2(d)). It can be observed that the measurements of $r_{2|2}$ generally deviate from unity and this deviation is stronger in most central and peripheral collisions, while it is less pronounced in midcentral collisions, in line with dominant average elliptic geometry at these collision centralities.

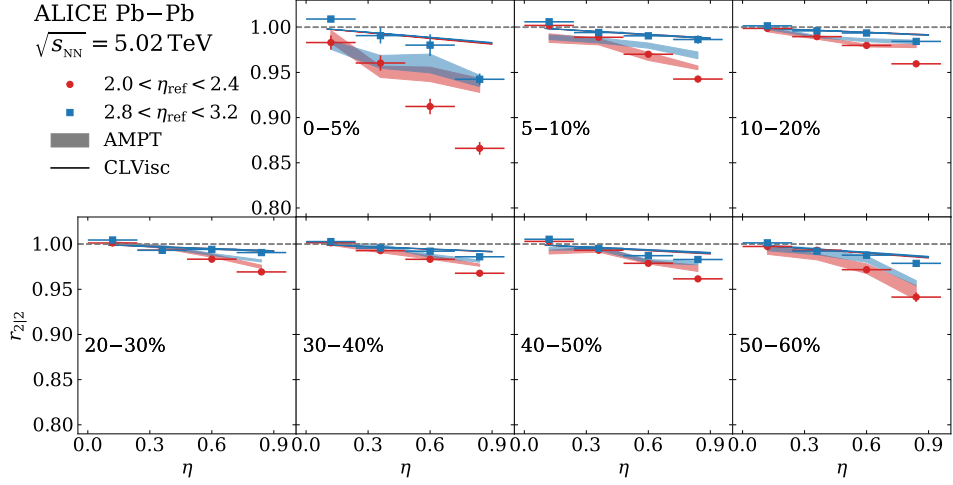


Figure 9: $r_{2|2}$ with different choices for of reference region η in Pb–Pb collisions at $\sqrt{s_{\text{NN}}} = 5.02$ TeV. AMPT and CLVisc model calculations are compared with the results.

Two perspectives of flow vector fluctuations can be studied from Fig. 9. First, for fixed η_{ref} , when η increases, the longitudinal decorrelation between two narrow intervals of POI, η and $-\eta$ is studied. At $\eta \sim 0$ (i.e. no relative separation), the correlations in both numerator and denominator of $r_{2|2}$ have similar longitudinal separation with respect to η_{ref} , therefore any effects arising from this η -gap cancel out in the $r_{2|2}$ ratio. On the contrary, the $r_{2|2}$ measurements at $\eta \sim 1.0$ have a large η -gap between correlated hadrons in the numerator ($|\eta - \eta_{\text{ref}}|$), and a small η -gap in the denominator ($|\eta - \eta_{\text{ref}}|$), which in the presence of flow vector fluctuations would lead to $r_{2|2} < 1$. The results presented in Fig. 9 therefore suggest the presence of longitudinal flow vector fluctuations, in agreement with prior observations in Refs. [16–18].

Secondly, for fixed η of the POI, the evolution of flow vector fluctuations with pseudorapidity can be addressed by investigating different choices of η_{ref} . If the fluctuations increase linearly with pseudorapidity, then the decorrelation effect from the pseudorapidity separation $\eta - \eta_{\text{ref}}$ would cancel out in $r_{2|2}$, and $r_{2|2}$ will only reflect the decorrelation between η and $-\eta$. That is, a linear increase in fluctuations would lead to a $r_{2|2}$ ratio independent of the choice of η_{ref} . The measurements of $r_{2|2}$ shown in Fig. 9 however exhibit a significant difference for different choices of the reference region, with more distant η_{ref} showing smaller decorrelation. This suggests, that the effect of flow fluctuations saturates at a particular value of η -gap. In case of a distant η_{ref} , the numerator would reach a saturation point, while the η -gap in the denominator is insufficient to reach it. On the contrary, in case of a close η_{ref} , neither the numerator nor the denominator would reach the saturation point, resulting in larger deviation of $r_{2|2}$ from unity. Under this assumption, $r_{2|2} \sim 1$ in the limiting case when both numerator and denominator would have the η -gap large enough for the fluctuations effect to be saturated. Therefore, the fact that our results with large η_{ref} exhibit smaller, but still statistically significant, decorrelation effect, suggests that the limiting η -gap is in the range $|\Delta\eta| > 2$.

A similar dependence on η_{ref} was found in Refs. [16–18], where it was argued that the difference of $r_{2|2}$ from different η_{ref} configurations may alter the presence of short-range non-flow correlations, leading to stronger artificial deviation of $r_{2|2}$ from unity in case η_{ref} is positioned closer to midrapidity. However, the same analysis in the HIJING model [63], which does not include any collective motion (not shown in the article), demonstrated that even with modest η -gap, the non-flow contamination in both numerator

and denominator of $r_{n|n}$ in heavy-ion collisions is negligible. In addition, non-flow effects tend to be more dominant in peripheral collisions, in contrast to the observations made in Fig. 9, where the largest difference of $r_{2|2}$ from different η_{ref} configurations was found in the most central collisions. The difference between the measurements with respect to the two η_{ref} regions seen in Fig. 9, therefore, cannot be explained solely by non-flow effects, and the deviation of $r_{2|2}$ from unity hints to sizable longitudinal flow vector fluctuations, which saturate at large pseudorapidity separations.

The measurements of $r_{3|3}$ in Pb–Pb collisions at $\sqrt{s_{\text{NN}}} = 5.02 \text{ TeV}$ are presented in Fig. 10 as a function of absolute η at different centrality classes, and for the two choices of the absolute η_{ref} regions. Results of $r_{3|3}$ for collision centralities larger than 40% are omitted due to large statistical uncertainties. Overall, $r_{3|3}$ shows a clear deviation from unity with larger magnitude than $r_{2|2}$. This observation is analogous to results presented in Ref. [16, 17] that included also the 4th harmonic, and is in line with expectations from fluctuation-driven harmonics of higher order. In addition, $r_{3|3}$ exhibits weaker centrality dependence as compared to $r_{2|2}$, similar to the observations of v_2 and v_3 coefficients shown in Figs. 3 and 4. Similarly as in Ref. [16, 17], measurements with different ranges of η_{ref} are compatible with each other within the statistical uncertainties, which suggest different η dependence of the longitudinal flow vector fluctuations compared with the $r_{2|2}$ measurement.

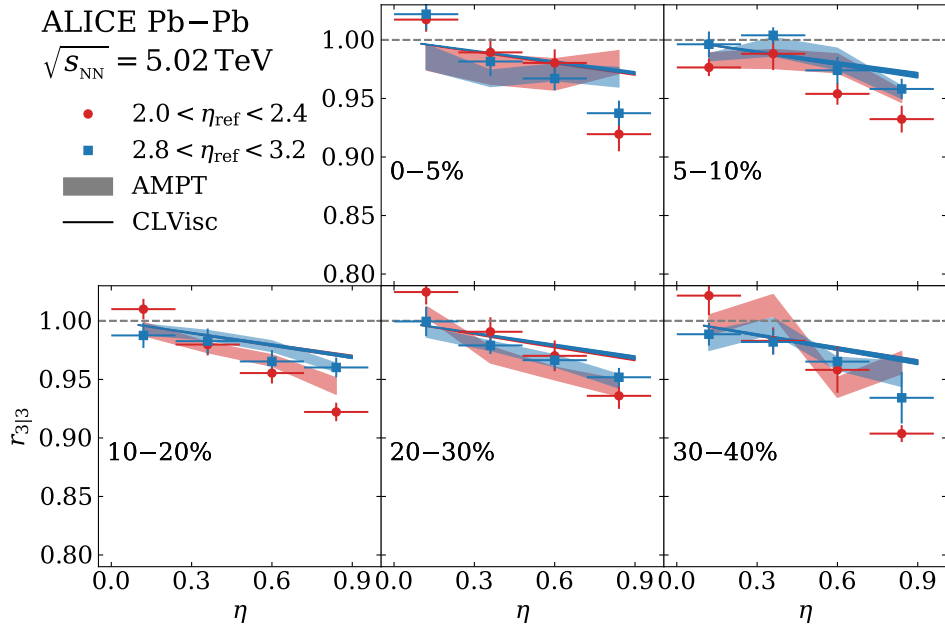


Figure 10: $r_{3|3}$ with different choices for reference region η in Pb–Pb collisions at $\sqrt{s_{\text{NN}}} = 5.02 \text{ TeV}$. AMPT and CLVisc model calculations are compared with the results.

Results presented in Figs. 9 and 10 are compared with the AMPT and CLVisc model calculations. As opposed to the measurements, the models do not distinguish between the choices of the η_{ref} regions used for correlations. This substantiates the observation that the deviation from unity is not driven by short range correlations. In case of $2.8 < |\eta_{\text{ref}}| < 3.2$, both models reproduce the trend of the data within uncertainties. On the contrary, when the reference region is chosen as $2.0 < |\eta_{\text{ref}}| < 2.4$, the CLVisc significantly underestimates the effect of longitudinal flow fluctuations, while AMPT reproduces the trend of the data except for the 5% most central collisions. Both models are able to reproduce the magnitude and trend of decorrelation of the $r_{3|3}$ results shown in Fig. 10 within the uncertainties.

6 Summary

The pseudorapidity and centrality dependence of v_2 , v_3 , and v_4 in both Pb–Pb at $\sqrt{s_{\text{NN}}} = 5.02 \text{ TeV}$ and Xe–Xe at $\sqrt{s_{\text{NN}}} = 5.44 \text{ TeV}$ is measured over the widest possible longitudinal range. The results show a smooth pseudorapidity dependence modulated by a strong collision centrality dependence. Non-flow contributions are minimised by using a pseudorapidity gap $|\Delta\eta| > 2$ or by using four-particle cumulants. The ratio of the second order flow coefficient calculated with four-particle cumulant ($v_2\{4, |\Delta\eta| > 0\}$) to the one obtained with two-particle cumulant with a large η -gap ($v_2\{2, |\Delta\eta| > 2, 3.8\}$) is almost constant over the whole pseudorapidity range. This result suggests that the variance of flow probability density function is independent of pseudorapidity, providing constraints to the models of fluctuating initial state. The longitudinal flow vector fluctuations are investigated via the measurements of the ratio $r_{n|n}$ to further quantify this observation. The $r_{2|2}$ exhibits a clear deviation from unity, which is more pronounced in central than peripheral collisions. The difference between the measured decorrelation with respect to different η_{ref} regions points to potential saturation effect of longitudinal flow vector fluctuations above a certain pseudorapidity separation. This is in contrast to current understanding based on previous publications at the LHC. The $r_{3|3}$ measurements reveal the effect of flow vector fluctuations of stronger magnitude, but with a weaker centrality dependence, compared to $r_{2|2}$. This confirms the fluctuation-driven nature of higher order harmonics. Both the AMPT and the CLVisc models can qualitatively reproduce the experimental results of v_n , but differ in important details such as overall amplitude and exact pseudorapidity dependence, especially near midrapidity. The measurements of $r_{n|n}$ are qualitatively reproduced by both models, except for the dependence on the choice of the reference region η_{ref} of $r_{2|2}$, which was not observed in the model calculations. These findings reveal that the current state-of-the-art models are not able to simultaneously describe the pseudorapidity dependence of anisotropic flow and its fluctuations. Our results highlight the inadequacies in the current understanding of particle production, particularly in the longitudinal direction, and shall help to improve the modelling of longitudinal fluctuations of initial conditions and the subsequent system evolution.

Acknowledgements

The ALICE Collaboration would like to thank all its engineers and technicians for their invaluable contributions to the construction of the experiment and the CERN accelerator teams for the outstanding performance of the LHC complex. The ALICE Collaboration gratefully acknowledges the resources and support provided by all Grid centres and the Worldwide LHC Computing Grid (WLCG) collaboration. The ALICE Collaboration acknowledges the following funding agencies for their support in building and running the ALICE detector: A. I. Alikhanyan National Science Laboratory (Yerevan Physics Institute) Foundation (ANSL), State Committee of Science and World Federation of Scientists (WFS), Armenia; Austrian Academy of Sciences, Austrian Science Fund (FWF): [M 2467-N36] and Nationalstiftung für Forschung, Technologie und Entwicklung, Austria; Ministry of Communications and High Technologies, National Nuclear Research Center, Azerbaijan; Conselho Nacional de Desenvolvimento Científico e Tecnológico (CNPq), Financiadora de Estudos e Projetos (Finep), Fundação de Amparo à Pesquisa do Estado de São Paulo (FAPESP) and Universidade Federal do Rio Grande do Sul (UFRGS), Brazil; Bulgarian Ministry of Education and Science, within the National Roadmap for Research Infrastructures 2020-2027 (object CERN), Bulgaria; Ministry of Education of China (MOEC) , Ministry of Science & Technology of China (MSTC) and National Natural Science Foundation of China (NSFC), China; Ministry of Science and Education and Croatian Science Foundation, Croatia; Centro de Aplicaciones Tecnológicas y Desarrollo Nuclear (CEADEN), Cubaenergía, Cuba; Ministry of Education, Youth and Sports of the Czech Republic, Czech Republic; The Danish Council for Independent Research | Natural Sciences, the VILLUM FONDEN and Danish National Research Foundation (DNRF), Denmark; Helsinki Institute of Physics (HIP), Finland; Commissariat à l’Energie Atomique (CEA) and Institut National de Physique Nucléaire et de Physique des Particules (IN2P3) and Centre National de la

Recherche Scientifique (CNRS), France; Bundesministerium für Bildung und Forschung (BMBF) and GSI Helmholtzzentrum für Schwerionenforschung GmbH, Germany; General Secretariat for Research and Technology, Ministry of Education, Research and Religions, Greece; National Research, Development and Innovation Office, Hungary; Department of Atomic Energy Government of India (DAE), Department of Science and Technology, Government of India (DST), University Grants Commission, Government of India (UGC) and Council of Scientific and Industrial Research (CSIR), India; National Research and Innovation Agency - BRIN, Indonesia; Istituto Nazionale di Fisica Nucleare (INFN), Italy; Japanese Ministry of Education, Culture, Sports, Science and Technology (MEXT) and Japan Society for the Promotion of Science (JSPS) KAKENHI, Japan; Consejo Nacional de Ciencia (CONACYT) y Tecnología, through Fondo de Cooperación Internacional en Ciencia y Tecnología (FONCICYT) and Dirección General de Asuntos del Personal Académico (DGAPA), Mexico; Nederlandse Organisatie voor Wetenschappelijk Onderzoek (NWO), Netherlands; The Research Council of Norway, Norway; Commission on Science and Technology for Sustainable Development in the South (COMSATS), Pakistan; Pontificia Universidad Católica del Perú, Peru; Ministry of Education and Science, National Science Centre and WUT ID-UB, Poland; Korea Institute of Science and Technology Information and National Research Foundation of Korea (NRF), Republic of Korea; Ministry of Education and Scientific Research, Institute of Atomic Physics, Ministry of Research and Innovation and Institute of Atomic Physics and Universitatea Națională de Știință și Tehnologie Politehnica București, Romania Ministry of Education, Science, Research and Sport of the Slovak Republic, Slovakia; National Research Foundation of South Africa, South Africa; Swedish Research Council (VR) and Knut & Alice Wallenberg Foundation (KAW), Sweden; European Organization for Nuclear Research, Switzerland; Suranaree University of Technology (SUT), National Science and Technology Development Agency (NSTDA) and National Science, Research and Innovation Fund (NSRF via PMU-B B05F650021), Thailand; Turkish Energy, Nuclear and Mineral Research Agency (TENMAK), Turkey; National Academy of Sciences of Ukraine, Ukraine; Science and Technology Facilities Council (STFC), United Kingdom; National Science Foundation of the United States of America (NSF) and United States Department of Energy, Office of Nuclear Physics (DOE NP), United States of America. In addition, individual groups or members have received support from: European Research Council, Strong 2020 - Horizon 2020 (grant nos. 950692, 824093), European Union; Academy of Finland (Center of Excellence in Quark Matter) (grant nos. 346327, 346328), Finland.

References

- [1] **BRAHMS** Collaboration, I. Arsene *et al.*, “Quark gluon plasma and color glass condensate at RHIC? The Perspective from the BRAHMS experiment”, *Nucl. Phys. A* **757** (2005) 1–27, [arXiv:nucl-ex/0410020](https://arxiv.org/abs/nucl-ex/0410020).
- [2] **PHOBOS** Collaboration, B. B. Back *et al.*, “The PHOBOS perspective on discoveries at RHIC”, *Nucl. Phys. A* **757** (2005) 28–101, [arXiv:nucl-ex/0410022](https://arxiv.org/abs/nucl-ex/0410022).
- [3] **STAR** Collaboration, J. Adams *et al.*, “Experimental and theoretical challenges in the search for the quark gluon plasma: The STAR Collaboration’s critical assessment of the evidence from RHIC collisions”, *Nucl. Phys. A* **757** (2005) 102–183, [arXiv:nucl-ex/0501009](https://arxiv.org/abs/nucl-ex/0501009).
- [4] **PHENIX** Collaboration, K. Adcox *et al.*, “Formation of dense partonic matter in relativistic nucleus-nucleus collisions at RHIC: Experimental evaluation by the PHENIX collaboration”, *Nucl. Phys. A* **757** (2005) 184–283, [arXiv:nucl-ex/0410003](https://arxiv.org/abs/nucl-ex/0410003).
- [5] **ALICE** Collaboration, “The ALICE experiment – A journey through QCD”, [arXiv:2211.04384 \[nucl-ex\]](https://arxiv.org/abs/2211.04384).

- [6] J.-Y. Ollitrault, “Anisotropy as a signature of transverse collective flow”, *Phys. Rev. D* **46** (1992) 229–245.
- [7] S. Voloshin and Y. Zhang, “Flow study in relativistic nuclear collisions by Fourier expansion of Azimuthal particle distributions”, *Z. Phys. C* **70** (1996) 665–672, arXiv:hep-ph/9407282.
- [8] F. G. Gardim, F. Grassi, M. Luzum, and J.-Y. Ollitrault, “Breaking of factorization of two-particle correlations in hydrodynamics”, *Phys. Rev. C* **87** (2013) 031901, arXiv:1211.0989 [nucl-th].
- [9] U. Heinz, Z. Qiu, and C. Shen, “Fluctuating flow angles and anisotropic flow measurements”, *Phys. Rev. C* **87** (2013) 034913, arXiv:1302.3535 [nucl-th].
- [10] U. Heinz and R. Snellings, “Collective flow and viscosity in relativistic heavy-ion collisions”, *Ann. Rev. Nucl. Part. Sci.* **63** (2013) 123–151, arXiv:1301.2826 [nucl-th].
- [11] M. Luzum and H. Petersen, “Initial State Fluctuations and Final State Correlations in Relativistic Heavy-Ion Collisions”, *J. Phys. G* **41** (2014) 063102, arXiv:1312.5503 [nucl-th].
- [12] E. Shuryak, “Strongly coupled quark-gluon plasma in heavy ion collisions”, *Rev. Mod. Phys.* **89** (2017) 035001, arXiv:1412.8393 [hep-ph].
- [13] H. Song, Y. Zhou, and K. Gajdosova, “Collective flow and hydrodynamics in large and small systems at the LHC”, *Nucl. Sci. Tech.* **28** (2017) 99, arXiv:1703.00670 [nucl-th].
- [14] P. Kovtun, D. T. Son, and A. O. Starinets, “Viscosity in strongly interacting quantum field theories from black hole physics”, *Phys. Rev. Lett.* **94** (2005) 111601, arXiv:hep-th/0405231 [hep-th].
- [15] **ALICE** Collaboration, S. Acharya *et al.*, “Searches for transverse momentum dependent flow vector fluctuations in Pb-Pb and p-Pb collisions at the LHC”, *JHEP* **09** (2017) 032, arXiv:1707.05690 [nucl-ex].
- [16] **CMS** Collaboration, V. Khachatryan *et al.*, “Evidence for transverse momentum and pseudorapidity dependent event plane fluctuations in PbPb and pPb collisions”, *Phys. Rev. C* **92** (2015) 034911, arXiv:1503.01692 [nucl-ex].
- [17] **ATLAS** Collaboration, M. Aaboud *et al.*, “Measurement of longitudinal flow decorrelations in Pb+Pb collisions at $\sqrt{s_{\text{NN}}} = 2.76$ and 5.02 TeV with the ATLAS detector”, *Eur. Phys. J. C* **78** (2018) 142, arXiv:1709.02301 [nucl-ex].
- [18] **ATLAS** Collaboration, G. Aad *et al.*, “Longitudinal Flow Decorrelations in Xe+Xe Collisions at $\sqrt{s_{\text{NN}}} = 5.44$ TeV with the ATLAS Detector”, *Phys. Rev. Lett.* **126** (2021) 122301, arXiv:2001.04201 [nucl-ex].
- [19] J. Jia and P. Huo, “Forward-backward eccentricity and participant-plane angle fluctuations and their influences on longitudinal dynamics of collective flow”, *Phys. Rev. C* **90** (2014) 034915, arXiv:1403.6077 [nucl-th].
- [20] P. Bozek and W. Broniowski, “The torque effect and fluctuations of entropy deposition in rapidity in ultra-relativistic nuclear collisions”, *Phys. Lett. B* **752** (2016) 206–211, arXiv:1506.02817 [nucl-th].
- [21] L.-G. Pang, H. Petersen, G.-Y. Qin, V. Roy, and X.-N. Wang, “Decorrelation of anisotropic flow along the longitudinal direction”, *Eur. Phys. J. A* **52** (2016) 97, arXiv:1511.04131 [nucl-th].

- [22] P. Bozek and W. Broniowski, “Longitudinal decorrelation measures of flow magnitude and event-plane angles in ultrarelativistic nuclear collisions”, *Phys. Rev. C* **97** (2018) 034913, arXiv:1711.03325 [nucl-th].
- [23] K. Xiao, F. Liu, and F. Wang, “Event-plane decorrelation over pseudorapidity and its effect on azimuthal anisotropy measurements in relativistic heavy-ion collisions”, *Phys. Rev. C* **87** (2013) 011901, arXiv:1208.1195 [nucl-th].
- [24] A. Sakai, K. Murase, and T. Hirano, “Rapidity decorrelation of anisotropic flow caused by hydrodynamic fluctuations”, *Phys. Rev. C* **102** (2020) 064903, arXiv:2003.13496 [nucl-th].
- [25] G. Denicol, A. Monnai, and B. Schenke, “Moving forward to constrain the shear viscosity of QCD matter”, *Phys. Rev. Lett.* **116** (2016) 212301, arXiv:1512.01538 [nucl-th].
- [26] E. Molnar, H. Holopainen, P. Huovinen, and H. Niemi, “Influence of temperature-dependent shear viscosity on elliptic flow at backward and forward rapidities in ultrarelativistic heavy-ion collisions”, *Phys. Rev. C* **90** (2014) 044904, arXiv:1407.8152 [nucl-th].
- [27] C. Shen and B. Schenke, “Dynamical initial state model for relativistic heavy-ion collisions”, *Phys. Rev. C* **97** (2018) 024907, arXiv:1710.00881 [nucl-th].
- [28] K. J. Eskola, H. Niemi, R. Paatelainen, and K. Tuominen, “Predictions for multiplicities and flow harmonics in 5.44 TeV Xe+Xe collisions at the CERN Large Hadron Collider”, *Phys. Rev. C* **97** (2018) 034911, arXiv:1711.09803 [hep-ph].
- [29] G. Giacalone, J. Noronha-Hostler, M. Luzum, and J.-Y. Ollitrault, “Hydrodynamic predictions for 5.44 TeV Xe+Xe collisions”, *Phys. Rev. C* **97** (2018) 034904, arXiv:1711.08499 [nucl-th].
- [30] **ALICE** Collaboration, S. Acharya *et al.*, “Anisotropic flow in Xe-Xe collisions at $\sqrt{s_{\text{NN}}} = 5.44$ TeV”, *Phys. Lett. B* **784** (2018) 82–95, arXiv:1805.01832 [nucl-ex].
- [31] N. Borghini, P. M. Dinh, and J.-Y. Ollitrault, “A New method for measuring azimuthal distributions in nucleus-nucleus collisions”, *Phys. Rev. C* **63** (2001) 054906, arXiv:nucl-th/0007063.
- [32] A. Bilandzic, C. H. Christensen, K. Gulbrandsen, A. Hansen, and Y. Zhou, “Generic framework for anisotropic flow analyses with multiparticle azimuthal correlations”, *Phys. Rev. C* **89** (2014) 064904, arXiv:1312.3572 [nucl-ex].
- [33] **CMS** Collaboration, A. M. Sirunyan *et al.*, “Pseudorapidity and transverse momentum dependence of flow harmonics in pPb and PbPb collisions”, *Phys. Rev. C* **98** (2018) 044902, arXiv:1710.07864 [nucl-ex].
- [34] **ALICE** Collaboration, J. Adam *et al.*, “Pseudorapidity dependence of the anisotropic flow of charged particles in Pb-Pb collisions at $\sqrt{s_{\text{NN}}} = 2.76$ TeV”, *Phys. Lett. B* **762** (2016) 376–388, arXiv:1605.02035 [nucl-ex].
- [35] X.-Y. Wu, L.-G. Pang, G.-Y. Qin, and X.-N. Wang, “Longitudinal fluctuations and decorrelations of anisotropic flows at energies available at the CERN Large Hadron Collider and at the BNL Relativistic Heavy Ion Collider”, *Phys. Rev. C* **98** (2018) 024913, arXiv:1805.03762 [nucl-th].
- [36] Z.-W. Lin, C. M. Ko, B.-A. Li, B. Zhang, and S. Pal, “A Multi-phase transport model for relativistic heavy ion collisions”, *Phys. Rev. C* **72** (2005) 064901, arXiv:nucl-th/0411110.

- [37] J. Jia, M. Zhou, and A. Trzupek, “Revealing long-range multiparticle collectivity in small collision systems via subevent cumulants”, *Phys. Rev. C* **96** (2017) 034906, arXiv:1701.03830 [nucl-th].
- [38] P. Huo, K. Gajdošová, J. Jia, and Y. Zhou, “Importance of non-flow in mixed-harmonic multi-particle correlations in small collision systems”, *Phys. Lett. B* **777** (2018) 201–206, arXiv:1710.07567 [nucl-ex].
- [39] ALICE Collaboration, K. Aamodt *et al.*, “The ALICE experiment at the CERN LHC”, *JINST* **3** (2008) S08002.
- [40] ALICE Collaboration, B. B. Abelev *et al.*, “Performance of the ALICE Experiment at the CERN LHC”, *Int. J. Mod. Phys. A* **29** (2014) 1430044, arXiv:1402.4476 [nucl-ex].
- [41] ALICE Collaboration, K. Aamodt *et al.*, “Alignment of the ALICE Inner Tracking System with cosmic-ray tracks”, *JINST* **5** (2010) P03003, arXiv:1001.0502 [physics.ins-det].
- [42] J. Alme *et al.*, “The ALICE TPC, a large 3-dimensional tracking device with fast readout for ultra-high multiplicity events”, *Nucl. Instrum. Meth. A* **622** (2010) 316–367, arXiv:1001.1950 [physics.ins-det].
- [43] ALICE Collaboration, P. Cortese *et al.*, “ALICE technical design report on forward detectors: FMD, T0 and V0”, CERN-LHCC-2004-025. <https://cds.cern.ch/record/781854>.
- [44] ALICE Collaboration, E. Abbas *et al.*, “Performance of the ALICE VZERO system”, *JINST* **8** (2013) P10016, arXiv:1306.3130 [nucl-ex].
- [45] ALICE Collaboration, J. Adam *et al.*, “Centrality evolution of the charged-particle pseudorapidity density over a broad pseudorapidity range in Pb-Pb collisions at $\sqrt{s_{NN}} = 2.76$ TeV”, *Phys. Lett. B* **754** (2016) 373–385, arXiv:1509.07299 [nucl-ex].
- [46] ALICE Collaboration, S. Acharya *et al.*, “The ALICE definition of primary particles”, ALICE-PUBLIC-2017-005. <https://cds.cern.ch/record/2270008>.
- [47] ALICE Collaboration, B. Abelev *et al.*, “Centrality determination of Pb-Pb collisions at $\sqrt{s_{NN}} = 2.76$ TeV with ALICE”, *Phys. Rev. C* **88** (2013) 044909, arXiv:1301.4361 [nucl-ex].
- [48] ALICE Collaboration, “Centrality determination in heavy ion collisions”, ALICE-PUBLIC-2018-011. <https://cds.cern.ch/record/2636623>.
- [49] ALICE Collaboration, S. Acharya *et al.*, “Centrality and pseudorapidity dependence of the charged-particle multiplicity density in Xe-Xe collisions at $\sqrt{s_{NN}} = 5.44$ TeV”, *Phys. Lett. B* **790** (2019) 35–48, arXiv:1805.04432 [nucl-ex].
- [50] ALICE Collaboration, J. Adam *et al.*, “Anisotropic flow of charged particles in Pb-Pb collisions at $\sqrt{s_{NN}} = 5.02$ TeV”, *Phys. Rev. Lett.* **116** (2016) 132302, arXiv:1602.01119 [nucl-ex].
- [51] S. A. Voloshin, A. M. Poskanzer, A. Tang, and G. Wang, “Elliptic flow in the Gaussian model of eccentricity fluctuations”, *Phys. Lett. B* **659** (2008) 537–541, arXiv:0708.0800 [nucl-th].
- [52] L. Yan and J.-Y. Ollitrault, “Universal fluctuation-driven eccentricities in proton-proton, proton-nucleus and nucleus-nucleus collisions”, *Phys. Rev. Lett.* **112** (2014) 082301, arXiv:1312.6555 [nucl-th].
- [53] L. Yan, J.-Y. Ollitrault, and A. M. Poskanzer, “Eccentricity distributions in nucleus-nucleus collisions”, *Phys. Rev. C* **90** (2014) 024903, arXiv:1405.6595 [nucl-th].

- [54] H. Grönqvist, J.-P. Blaizot, and J.-Y. Ollitrault, “Non-Gaussian eccentricity fluctuations”, *Phys. Rev. C* **94** (2016) 034905, arXiv:1604.07230 [nucl-th].
- [55] H. Holopainen, H. Niemi, and K. J. Eskola, “Event-by-event hydrodynamics and elliptic flow from fluctuating initial state”, *Phys. Rev. C* **83** (2011) 034901, arXiv:1007.0368 [hep-ph].
- [56] G.-Y. Qin, H. Petersen, S. A. Bass, and B. Muller, “Translation of collision geometry fluctuations into momentum anisotropies in relativistic heavy-ion collisions”, *Phys. Rev. C* **82** (2010) 064903, arXiv:1009.1847 [nucl-th].
- [57] Z. Qiu and U. W. Heinz, “Event-by-event shape and flow fluctuations of relativistic heavy-ion collision fireballs”, *Phys. Rev. C* **84** (2011) 024911, arXiv:1104.0650 [nucl-th].
- [58] C. Gale, S. Jeon, B. Schenke, P. Tribedy, and R. Venugopalan, “Event-by-event anisotropic flow in heavy-ion collisions from combined Yang-Mills and viscous fluid dynamics”, *Phys. Rev. Lett.* **110** (2013) 012302, arXiv:1209.6330 [nucl-th].
- [59] H. Niemi, G. S. Denicol, H. Holopainen, and P. Huovinen, “Event-by-event distributions of azimuthal asymmetries in ultrarelativistic heavy-ion collisions”, *Phys. Rev. C* **87** (2013) 054901, arXiv:1212.1008 [nucl-th].
- [60] ALICE Collaboration, S. Acharya *et al.*, “Energy dependence and fluctuations of anisotropic flow in Pb-Pb collisions at $\sqrt{s_{\text{NN}}} = 5.02$ and 2.76 TeV”, *JHEP* **07** (2018) 103, arXiv:1804.02944 [nucl-ex].
- [61] CMS Collaboration, A. M. Sirunyan *et al.*, “Charged-particle angular correlations in XeXe collisions at $\sqrt{s_{\text{NN}}} = 5.44$ TeV”, *Phys. Rev. C* **100** (2019) 044902, arXiv:1901.07997 [hep-ex].
- [62] G.-L. Ma and Z.-W. Lin, “Predictions for $\sqrt{s_{\text{NN}}} = 5.02$ TeV Pb+Pb Collisions from a Multi-Phase Transport Model”, *Phys. Rev. C* **93** (2016) 054911, arXiv:1601.08160 [nucl-th].
- [63] M. Gyulassy and X.-N. Wang, “HIJING 1.0: A Monte Carlo program for parton and particle production in high-energy hadronic and nuclear collisions”, *Comput. Phys. Commun.* **83** (1994) 307, arXiv:nucl-th/9502021 [nucl-th].

A The ALICE Collaboration

S. Acharya ¹²⁸, D. Adamová ⁸⁷, A. Adler ⁷¹, G. Aglieri Rinella ³³, M. Agnello ³⁰, N. Agrawal ⁵², Z. Ahammed ¹³⁶, S. Ahmad ¹⁶, S.U. Ahn ⁷², I. Ahuja ³⁸, A. Akindinov ¹⁴², M. Al-Turany ⁹⁸, D. Aleksandrov ¹⁴², B. Alessandro ⁵⁷, H.M. Alfanda ⁶, R. Alfaro Molina ⁶⁸, B. Ali ¹⁶, A. Alici ²⁶, N. Alizadehvandchali ¹¹⁷, A. Alkin ³³, J. Alme ²¹, G. Alocco ⁵³, T. Alt ⁶⁵, A.R. Altamura ⁵¹, I. Altsybeev ⁹⁶, J.R. Alvarado ⁴⁵, M.N. Anaam ⁶, C. Andrei ⁴⁶, N. Andreou ¹¹⁶, A. Andronic ¹²⁷, V. Anguelov ⁹⁵, F. Antinori ⁵⁵, P. Antonioli ⁵², N. Apadula ⁷⁵, L. Aphecetche ¹⁰⁴, H. Appelshäuser ⁶⁵, C. Arata ⁷⁴, S. Arcelli ²⁶, M. Aresti ²³, R. Arnaldi ⁵⁷, J.G.M.C.A. Arneiro ¹¹¹, I.C. Arsene ²⁰, M. Arslanbek ¹³⁹, A. Augustinus ³³, R. Averbeck ⁹⁸, M.D. Azmi ¹⁶, H. Baba ¹²⁵, A. Badalà ⁵⁴, J. Bae ¹⁰⁵, Y.W. Baek ⁴¹, X. Bai ¹²¹, R. Bailhache ⁶⁵, Y. Bailung ⁴⁹, A. Balbino ³⁰, A. Baldissari ¹³¹, B. Balis ², D. Banerjee ⁴, Z. Banoo ⁹², R. Barbera ²⁷, F. Barile ³², L. Barioglio ⁹⁶, M. Barlou ⁷⁹, G.G. Barnaföldi ⁴⁷, L.S. Barnby ⁸⁶, V. Barret ¹²⁸, L. Barreto ¹¹¹, C. Bartels ¹²⁰, K. Barth ³³, E. Bartsch ⁶⁵, N. Bastid ¹²⁸, S. Basu ⁷⁶, G. Batigne ¹⁰⁴, D. Battistini ⁹⁶, B. Batyunya ¹⁴³, D. Bauri ⁴⁸, J.L. Bazo Alba ¹⁰², I.G. Bearden ⁸⁴, C. Beattie ¹³⁹, P. Becht ⁹⁸, D. Behera ⁴⁹, I. Belikov ¹³⁰, A.D.C. Bell Hechavarria ¹²⁷, F. Bellini ²⁶, R. Bellwied ¹¹⁷, S. Belokurova ¹⁴², G. Bencedi ⁴⁷, S. Beole ²⁵, Y. Berdnikov ¹⁴², A. Berdnikova ⁹⁵, L. Bergmann ⁹⁵, M.G. Besouï ⁶⁴, L. Betev ³³, P.P. Bhaduri ¹³⁶, A. Bhasin ⁹², M.A. Bhat ⁴, B. Bhattacharjee ⁴², L. Bianchi ²⁵, N. Bianchi ⁵⁰, J. Bielčík ³⁶, J. Bielčíková ⁸⁷, J. Biernat ¹⁰⁸, A.P. Bigot ¹³⁰, A. Bilandzic ⁹⁶, G. Biro ⁴⁷, S. Biswas ⁴, N. Bize ¹⁰⁴, J.T. Blair ¹⁰⁹, D. Blau ¹⁴², M.B. Blidaru ⁹⁸, N. Bluhme ³⁹, C. Blume ⁶⁵, G. Boca ^{22,56}, F. Bock ⁸⁸, T. Bodova ²¹, A. Bogdanov ¹⁴², S. Boi ²³, J. Bok ⁵⁹, L. Boldziszár ⁴⁷, M. Bombara ³⁸, P.M. Bond ³³, G. Bonomi ^{135,56}, H. Borel ¹³¹, A. Borissov ¹⁴², A.G. Borquez Carcamo ⁹⁵, H. Bossi ¹³⁹, E. Botta ²⁵, Y.E.M. Bouziani ⁶⁵, L. Bratrud ⁶⁵, P. Braun-Munzinger ⁹⁸, M. Bregant ¹¹¹, M. Broz ³⁶, G.E. Bruno ^{97,32}, M.D. Buckland ²⁴, D. Budnikov ¹⁴², H. Buesching ⁶⁵, S. Bufalino ³⁰, P. Buhler ¹⁰³, N. Burmasov ¹⁴², Z. Buthelezi ^{69,124}, A. Bylinkin ²¹, S.A. Bysiak ¹⁰⁸, M. Cai ⁶, H. Caines ¹³⁹, A. Caliva ²⁹, E. Calvo Villar ¹⁰², J.M.M. Camacho ¹¹⁰, P. Camerini ²⁴, F.D.M. Canedo ¹¹¹, S.L. Cantway ¹³⁹, M. Carabas ¹¹⁴, A.A. Carballo ³³, F. Carnesecchi ³³, R. Caron ¹²⁹, L.A.D. Carvalho ¹¹¹, J. Castillo Castellanos ¹³¹, F. Catalano ^{33,25}, C. Ceballos Sanchez ¹⁴³, I. Chakaberia ⁷⁵, P. Chakraborty ⁴⁸, S. Chandra ¹³⁶, S. Chapeland ³³, M. Chartier ¹²⁰, S. Chattopadhyay ¹³⁶, S. Chattopadhyay ¹⁰⁰, T. Cheng ^{98,6}, C. Cheshkov ¹²⁹, B. Cheynis ¹²⁹, V. Chibante Barroso ³³, D.D. Chinellato ¹¹², E.S. Chizzali ^{II,96}, J. Cho ⁵⁹, S. Cho ⁵⁹, P. Chochula ³³, P. Christakoglou ⁸⁵, C.H. Christensen ⁸⁴, P. Christiansen ⁷⁶, T. Chujo ¹²⁶, M. Ciaccio ³⁰, C. Cicalo ⁵³, F. Cindolo ⁵², M.R. Ciupek ⁹⁸, G. Clai^{III,52}, F. Colamaria ⁵¹, J.S. Colburn ¹⁰¹, D. Colella ^{97,32}, M. Colocci ²⁶, M. Concas ^{IV,57}, G. Conesa Balbastre ⁷⁴, Z. Conesa del Valle ¹³², G. Contin ²⁴, J.G. Contreras ³⁶, M.L. Coquet ¹³¹, P. Cortese ^{134,57}, M.R. Cosentino ¹¹³, F. Costa ³³, S. Costanza ^{22,56}, C. Cot ¹³², J. Crkovská ⁹⁵, P. Crochet ¹²⁸, R. Cruz-Torres ⁷⁵, P. Cui ⁶, A. Dainese ⁵⁵, M.C. Danisch ⁹⁵, A. Danu ⁶⁴, P. Das ⁸¹, P. Das ⁴, S. Das ⁴, A.R. Dash ¹²⁷, S. Dash ⁴⁸, A. De Caro ²⁹, G. de Cataldo ⁵¹, J. de Cuveland ³⁹, A. De Falco ²³, D. De Gruttola ²⁹, N. De Marco ⁵⁷, C. De Martin ²⁴, S. De Pasquale ²⁹, R. Deb ¹³⁵, R. Del Grande ⁹⁶, L. Dello Stritto ²⁹, W. Deng ⁶, P. Dhankher ¹⁹, D. Di Bari ³², A. Di Mauro ³³, B. Diab ¹³¹, R.A. Diaz ^{143,7}, T. Dietel ¹¹⁵, Y. Ding ⁶, R. Divià ³³, D.U. Dixit ¹⁹, Ø. Djupsland ²¹, U. Dmitrieva ¹⁴², A. Dobrin ⁶⁴, B. Dönigus ⁶⁵, J.M. Dubinski ¹³⁷, A. Dubla ⁹⁸, S. Dudi ⁹¹, P. Dupieux ¹²⁸, M. Durkac ¹⁰⁷, N. Dzalaiova ¹³, T.M. Eder ¹²⁷, R.J. Ehlers ⁷⁵, F. Eisenhut ⁶⁵, R. Ejima ⁹³, D. Elia ⁵¹, B. Erazmus ¹⁰⁴, F. Ercolelli ²⁶, F. Erhardt ⁹⁰, M.R. Ersdal ²¹, B. Espagnon ¹³², G. Eulisse ³³, D. Evans ¹⁰¹, S. Evdokimov ¹⁴², L. Fabbietti ⁹⁶, M. Faggin ²⁸, J. Faivre ⁷⁴, F. Fan ⁶, W. Fan ⁷⁵, A. Fantoni ⁵⁰, M. Fasel ⁸⁸, P. Fecchio ³⁰, A. Feliciello ⁵⁷, G. Feofilov ¹⁴², A. Fernández Téllez ⁴⁵, L. Ferrandi ¹¹¹, M.B. Ferrer ³³, A. Ferrero ¹³¹, C. Ferrero ⁵⁷, A. Ferretti ²⁵, V.J.G. Feuillard ⁹⁵, V. Filova ³⁶, D. Finogeev ¹⁴², F.M. Fionda ⁵³, F. Flor ¹¹⁷, A.N. Flores ¹⁰⁹, S. Foertsch ⁶⁹, I. Fokin ⁹⁵, S. Fokin ¹⁴², E. Fragaicom ⁵⁸, E. Frajna ⁴⁷, U. Fuchs ³³, N. Funicello ²⁹, C. Furret ⁷⁴, A. Furs ¹⁴², T. Fusayasu ⁹⁹, J.J. Gaardhøje ⁸⁴, M. Gagliardi ²⁵, A.M. Gago ¹⁰², T. Gahlaud ⁴⁸, C.D. Galvan ¹¹⁰, D.R. Gangadharan ¹¹⁷, P. Ganoti ⁷⁹, C. Garabatos ⁹⁸, T. García Chávez ⁴⁵, E. Garcia-Solis ⁹, C. Gargiulo ³³, K. Garner ¹²⁷, P. Gasik ⁹⁸, A. Gautam ¹¹⁹, M.B. Gay Ducati ⁶⁷, M. Germain ¹⁰⁴, A. Ghimouz ¹²⁶, C. Ghosh ¹³⁶, M. Giacalone ⁵², G. Gioachin ³⁰, P. Giubellino ^{98,57}, P. Giubilato ²⁸, A.M.C. Glaenzer ¹³¹, P. Glässel ⁹⁵, E. Glimos ¹²³, D.J.Q. Goh ⁷⁷, V. Gonzalez ¹³⁸, M. Gorgon ², K. Goswami ⁴⁹, S. Gotovac ³⁴, V. Grabski ⁶⁸, L.K. Graczykowski ¹³⁷, E. Grecka ⁸⁷, A. Grelli ⁶⁰, C. Grigoras ³³, V. Grigoriev ¹⁴², S. Grigoryan ^{143,1}, F. Grossa ³³, J.F. Grosse-Oetringhaus ³³, R. Grossi ⁹⁸, D. Grund ³⁶, G.G. Guardiano ¹¹², R. Guernane ⁷⁴, M. Guilbaud ¹⁰⁴, K. Gulbrandsen ⁸⁴, T. Gündem ⁶⁵, T. Gunji ¹²⁵, W. Guo ⁶,

- A. Gupta ⁹², R. Gupta ⁹², R. Gupta ⁴⁹, K. Gwizdziel ¹³⁷, L. Gyulai ⁴⁷, C. Hadjidakis ¹³²,
 F.U. Haider ⁹², H. Hamagaki ⁷⁷, A. Hamdi ⁷⁵, Y. Han ¹⁴⁰, B.G. Hanley ¹³⁸, R. Hannigan ¹⁰⁹,
 J. Hansen ⁷⁶, M.R. Haque ¹³⁷, J.W. Harris ¹³⁹, A. Harton ⁹, H. Hassan ⁸⁸, D. Hatzifotiadou ⁵²,
 P. Hauer ⁴³, L.B. Havener ¹³⁹, S.T. Heckel ⁹⁶, E. Hellbär ⁹⁸, H. Helstrup ³⁵, M. Hemmer ⁶⁵,
 T. Herman ³⁶, G. Herrera Corral ⁸, F. Herrmann ¹²⁷, S. Herrmann ¹²⁹, K.F. Hetland ³⁵, B. Heybeck ⁶⁵,
 H. Hillemanns ³³, B. Hippolyte ¹³⁰, F.W. Hoffmann ⁷¹, B. Hofman ⁶⁰, G.H. Hong ¹⁴⁰, M. Horst ⁹⁶,
 A. Horzyk ², Y. Hou ⁶, P. Hristov ³³, C. Hughes ¹²³, P. Huhn ⁶⁵, L.M. Huhta ¹¹⁸, T.J. Humanic ⁸⁹,
 A. Hutson ¹¹⁷, D. Hutter ³⁹, R. Ilkaev ¹⁴², H. Ilyas ¹⁴, M. Inaba ¹²⁶, G.M. Innocenti ³³,
 M. Ippolitov ¹⁴², A. Isakov ^{85,87}, T. Isidori ¹¹⁹, M.S. Islam ¹⁰⁰, M. Ivanov ¹³, M. Ivanov ⁹⁸,
 V. Ivanov ¹⁴², K.E. Iversen ⁷⁶, M. Jablonski ², B. Jacak ⁷⁵, N. Jacazio ²⁶, P.M. Jacobs ⁷⁵,
 S. Jadlovska ¹⁰⁷, J. Jadlovsky ¹⁰⁷, S. Jaelani ⁸³, C. Jahnke ¹¹², M.J. Jakubowska ¹³⁷, M.A. Janik ¹³⁷,
 T. Janson ⁷¹, S. Ji ¹⁷, S. Jia ¹⁰, A.A.P. Jimenez ⁶⁶, F. Jonas ^{88,127}, D.M. Jones ¹²⁰, J.M. Jowett ^{33,98},
 J. Jung ⁶⁵, M. Jung ⁶⁵, A. Junique ³³, A. Jusko ¹⁰¹, M.J. Kabus ^{33,137}, J. Kaewjai ¹⁰⁶, P. Kalinak ⁶¹,
 A.S. Kalteyer ⁹⁸, A. Kalweit ³³, V. Kaplin ¹⁴², A. Karasu Uysal ⁷³, D. Karatovic ⁹⁰, O. Karavichev ¹⁴²,
 T. Karavicheva ¹⁴², P. Karczmarczyk ¹³⁷, E. Karpechev ¹⁴², U. Kebschull ⁷¹, R. Keidel ¹⁴¹,
 D.L.D. Keijdener ⁶⁰, M. Keil ³³, B. Ketzer ⁴³, S.S. Khade ⁴⁹, A.M. Khan ^{121,6}, S. Khan ¹⁶,
 A. Khanzadeev ¹⁴², Y. Kharlov ¹⁴², A. Khatun ¹¹⁹, A. Khuntia ³⁶, B. Kileng ³⁵, B. Kim ¹⁰⁵,
 C. Kim ¹⁷, D.J. Kim ¹¹⁸, E.J. Kim ⁷⁰, J. Kim ¹⁴⁰, J.S. Kim ⁴¹, J. Kim ⁵⁹, J. Kim ⁷⁰, M. Kim ¹⁹,
 S. Kim ¹⁸, T. Kim ¹⁴⁰, K. Kimura ⁹³, S. Kirsch ⁶⁵, I. Kisiel ³⁹, S. Kiselev ¹⁴², A. Kisiel ¹³⁷,
 J.P. Kitowski ², J.L. Klay ⁵, J. Klein ³³, S. Klein ⁷⁵, C. Klein-Bösing ¹²⁷, M. Kleiner ⁶⁵,
 T. Klemenz ⁹⁶, A. Kluge ³³, A.G. Knospe ¹¹⁷, C. Kobdaj ¹⁰⁶, T. Kollegger ⁹⁸, A. Kondratyev ¹⁴³,
 N. Kondratyeva ¹⁴², E. Kondratyuk ¹⁴², J. Konig ⁶⁵, S.A. Konigstorfer ⁹⁶, P.J. Konopka ³³,
 G. Kornakov ¹³⁷, M. Kowwieser ⁹⁶, S.D. Koryciak ², A. Kotliarov ⁸⁷, V. Kovalenko ¹⁴²,
 M. Kowalski ¹⁰⁸, V. Kozhuharov ³⁷, I. Králík ⁶¹, A. Kravčáková ³⁸, L. Krcal ^{33,39}, M. Krivda ^{101,61},
 F. Krizek ⁸⁷, K. Krizkova Gajdosova ³³, M. Kroesen ⁹⁵, M. Krüger ⁶⁵, D.M. Krupova ³⁶,
 E. Kryshen ¹⁴², V. Kučera ⁵⁹, C. Kuhn ¹³⁰, P.G. Kuijer ⁸⁵, T. Kumaoka ¹²⁶, D. Kumar ¹³⁶, L. Kumar ⁹¹,
 N. Kumar ⁹¹, S. Kumar ³², S. Kundu ³³, P. Kurashvili ⁸⁰, A. Kurepin ¹⁴², A.B. Kurepin ¹⁴²,
 A. Kuryakin ¹⁴², S. Kushpil ⁸⁷, M.J. Kweon ⁵⁹, Y. Kwon ¹⁴⁰, S.L. La Pointe ³⁹, P. La Rocca ²⁷,
 A. Lakrathok ¹⁰⁶, M. Lamanna ³³, A.R. Landou ^{74,116}, R. Langoy ¹²², P. Larionov ³³, E. Laudi ³³,
 L. Lautner ^{33,96}, R. Lavicka ¹⁰³, R. Lea ^{135,56}, H. Lee ¹⁰⁵, I. Legrand ⁴⁶, G. Legras ¹²⁷,
 J. Lehrbach ³⁹, T.M. Lelek ², R.C. Lemmon ⁸⁶, I. León Monzón ¹¹⁰, M.M. Lesch ⁹⁶, E.D. Lesser ¹⁹,
 P. Lévai ⁴⁷, X. Li ¹⁰, X.L. Li ⁶, J. Lien ¹²², R. Lietava ¹⁰¹, I. Likmeta ¹¹⁷, B. Lim ²⁵, S.H. Lim ¹⁷,
 V. Lindenstruth ³⁹, A. Lindner ⁴⁶, C. Lippmann ⁹⁸, A. Liu ¹⁹, D.H. Liu ⁶, J. Liu ¹²⁰, G.S.S. Liveraro ¹¹²,
 I.M. Lofnes ²¹, C. Loizides ⁸⁸, S. Lokos ¹⁰⁸, J. Lömkner ⁶⁰, P. Loncar ³⁴, X. Lopez ¹²⁸, E. López
 Torres ⁷, P. Lu ^{98,121}, J.R. Luhder ¹²⁷, M. Lunardon ²⁸, G. Luparello ⁵⁸, Y.G. Ma ⁴⁰, M. Mager ³³,
 A. Maire ¹³⁰, E.M. Majerz ², M.V. Makariev ³⁷, M. Malaev ¹⁴², G. Malfattore ²⁶, N.M. Malik ⁹²,
 Q.W. Malik ²⁰, S.K. Malik ⁹², L. Malinina ^{I,VII,143}, D. Mallick ^{132,81}, N. Mallick ⁴⁹, G. Mandaglio ^{31,54},
 S.K. Mandal ⁸⁰, V. Manko ¹⁴², F. Manso ¹²⁸, V. Manzari ⁵¹, Y. Mao ⁶, R.W. Marcjan ²,
 G.V. Margagliotti ²⁴, A. Margotti ⁵², A. Marín ⁹⁸, C. Markert ¹⁰⁹, P. Martinengo ³³, M.I. Martínez ⁴⁵,
 G. Martínez García ¹⁰⁴, M.P.P. Martins ¹¹¹, S. Masciocchi ⁹⁸, M. Masera ²⁵, A. Masoni ⁵³,
 L. Massacrier ¹³², O. Massen ⁶⁰, A. Mastroserio ^{133,51}, O. Matonoha ⁷⁶, S. Mattiuzzo ²⁸,
 P.F.T. Matuoka ¹¹¹, A. Matyja ¹⁰⁸, C. Mayer ¹⁰⁸, A.L. Mazuecos ³³, F. Mazzaschi ²⁵, M. Mazzilli ³³,
 J.E. Mdhluli ¹²⁴, A.F. Mechler ⁶⁵, Y. Melikyan ⁴⁴, A. Menchaca-Rocha ⁶⁸, E. Meninno ¹⁰³,
 A.S. Menon ¹¹⁷, M. Meres ¹³, S. Mhlanga ^{115,69}, Y. Miake ¹²⁶, L. Micheletti ³³, L.C. Migliorin ¹²⁹,
 D.L. Mihaylov ⁹⁶, K. Mikhaylov ^{143,142}, A.N. Mishra ⁴⁷, D. Miśkowiec ⁹⁸, A. Modak ⁴,
 A.P. Mohanty ⁶⁰, B. Mohanty ⁸¹, M. Mohisin Khan ^{V,16}, M.A. Molander ⁴⁴, S. Monira ¹³⁷,
 Z. Moravcova ⁸⁴, C. Mordasini ¹¹⁸, D.A. Moreira De Godoy ¹²⁷, I. Morozov ¹⁴², A. Morsch ³³,
 T. Mrnjavac ³³, V. Muccifora ⁵⁰, S. Muhuri ¹³⁶, J.D. Mulligan ⁷⁵, A. Mulliri ²³, M.G. Munhoz ¹¹¹,
 R.H. Munzer ⁶⁵, H. Murakami ¹²⁵, S. Murray ¹¹⁵, L. Musa ³³, J. Musinsky ⁶¹, J.W. Myrcha ¹³⁷,
 B. Naik ¹²⁴, A.I. Nambrath ¹⁹, B.K. Nandi ⁴⁸, R. Nania ⁵², E. Nappi ⁵¹, A.F. Nassirpour ^{18,76},
 A. Nath ⁹⁵, C. Nattrass ¹²³, M.N. Naydenov ³⁷, A. Neagu ²⁰, A. Negru ¹¹⁴, L. Nellen ⁶⁶, R. Nepeivoda ⁷⁶,
 S. Nese ²⁰, G. Neskovic ³⁹, N. Nicassio ⁵¹, B.S. Nielsen ⁸⁴, E.G. Nielsen ⁸⁴, S. Nikolaev ¹⁴²,
 S. Nikulin ¹⁴², V. Nikulin ¹⁴², F. Noferini ⁵², S. Noh ¹², P. Nomokonov ¹⁴³, J. Norman ¹²⁰,
 N. Novitzky ¹²⁶, P. Nowakowski ¹³⁷, A. Nyanin ¹⁴², J. Nystrand ²¹, M. Ogino ⁷⁷, S. Oh ¹⁸,
 A. Ohlson ⁷⁶, V.A. Okorokov ¹⁴², J. Oleniacz ¹³⁷, A.C. Oliveira Da Silva ¹²³, M.H. Oliver ¹³⁹,
 A. Onnerstad ¹¹⁸, C. Oppedisano ⁵⁷, A. Ortiz Velasquez ⁶⁶, J. Otwinowski ¹⁰⁸, M. Oya ⁹³, K. Oyama ⁷⁷,

- Y. Pachmayer ⁹⁵, S. Padhan ⁴⁸, D. Pagano ^{135,56}, G. Paić ⁶⁶, S. Paisano-Guzmán ⁴⁵, A. Palasciano ⁵¹,
 S. Panebianco ¹³¹, H. Park ¹²⁶, H. Park ¹⁰⁵, J. Park ⁵⁹, J.E. Parkkila ³³, Y. Patley ⁴⁸, R.N. Patra ⁹²,
 B. Paul ²³, H. Pei ⁶, T. Peitzmann ⁶⁰, X. Peng ¹¹, M. Pennisi ²⁵, S. Perciballi ²⁵, D. Peresunko ¹⁴²,
 G.M. Perez ⁷, Y. Pestov ¹⁴², V. Petrov ¹⁴², M. Petrovici ⁴⁶, R.P. Pezzi ^{104,67}, S. Piano ⁵⁸, M. Pikna ¹³,
 P. Pillot ¹⁰⁴, O. Pinazza ^{52,33}, L. Pinsky ¹¹⁷, C. Pinto ⁹⁶, S. Pisano ⁵⁰, M. Płoskoń ⁷⁵, M. Planinic ⁹⁰,
 F. Pliquet ⁶⁵, M.G. Poghosyan ⁸⁸, B. Polichtchouk ¹⁴², S. Politano ³⁰, N. Poljak ⁹⁰, A. Pop ⁴⁶,
 S. Porteboeuf-Houssais ¹²⁸, V. Pozdniakov ¹⁴³, I.Y. Pozos ⁴⁵, K.K. Pradhan ⁴⁹, S.K. Prasad ⁴,
 S. Prasad ⁴⁹, R. Preghenella ⁵², F. Prino ⁵⁷, C.A. Pruneau ¹³⁸, I. Pshenichnov ¹⁴², M. Puccio ³³,
 S. Pucillo ²⁵, Z. Pugelova ¹⁰⁷, S. Qiu ⁸⁵, L. Quaglia ²⁵, R.E. Quishpe ¹¹⁷, S. Ragoni ¹⁵, A. Rai ¹³⁹,
 A. Rakotozafindrabe ¹³¹, L. Ramello ^{134,57}, F. Rami ¹³⁰, T.A. Rancien ⁷⁴, M. Rasa ²⁷, S.S. Räsänen ⁴⁴,
 R. Rath ⁵², M.P. Rauch ²¹, I. Ravasenga ⁸⁵, K.F. Read ^{88,123}, C. Reckziegel ¹¹³, A.R. Redelbach ³⁹,
 K. Redlich ^{VI,80}, C.A. Reetz ⁹⁸, H.D. Regules-Medel ⁴⁵, A. Rehman ²¹, F. Reidt ³³, H.A. Reme-Ness ³⁵,
 Z. Rescakova ³⁸, K. Reygers ⁹⁵, A. Riabov ¹⁴², V. Riabov ¹⁴², R. Ricci ²⁹, M. Richter ²⁰,
 A.A. Riedel ⁹⁶, W. Riegler ³³, A.G. Rifferto ²⁵, C. Ristea ⁶⁴, M.V. Rodriguez ³³, M. Rodríguez
 Cahuantzi ⁴⁵, S.A. Rodríguez Ramírez ⁴⁵, K. Røed ²⁰, R. Rogalev ¹⁴², E. Rogochaya ¹⁴³,
 T.S. Rogoschinski ⁶⁵, D. Rohr ³³, D. Röhrlrich ²¹, P.F. Rojas ⁴⁵, S. Rojas Torres ³⁶, P.S. Rokita ¹³⁷,
 G. Romanenko ²⁶, F. Ronchetti ⁵⁰, A. Rosano ^{31,54}, E.D. Rosas ⁶⁶, K. Roslon ¹³⁷, A. Rossi ⁵⁵,
 A. Roy ⁴⁹, S. Roy ⁴⁸, N. Rubini ²⁶, D. Ruggiano ¹³⁷, R. Rui ²⁴, P.G. Russek ², R. Russo ⁸⁵,
 A. Rustamov ⁸², E. Ryabinkin ¹⁴², Y. Ryabov ¹⁴², A. Rybicki ¹⁰⁸, H. Rytkonen ¹¹⁸, J. Ryu ¹⁷,
 W. Rzesz ¹³⁷, O.A.M. Saarimaki ⁴⁴, S. Sadhu ³², S. Sadovsky ¹⁴², J. Saetre ²¹, K. Šafařík ³⁶, P. Saha ⁴²,
 S.K. Saha ⁴, S. Saha ⁸¹, B. Sahoo ⁴⁸, B. Sahoo ⁴⁹, R. Sahoo ⁴⁹, S. Sahoo ⁶², D. Sahu ⁴⁹, P.K. Sahu ⁶²,
 J. Saini ¹³⁶, K. Sajdakova ³⁸, S. Sakai ¹²⁶, M.P. Salvan ⁹⁸, S. Sambyal ⁹², D. Samitz ¹⁰³, I. Sanna ^{33,96},
 T.B. Saramela ¹¹¹, P. Sarma ⁴², V. Sarritzu ²³, V.M. Sarti ⁹⁶, M.H.P. Sas ¹³⁹, J. Schambach ⁸⁸,
 H.S. Scheid ⁶⁵, C. Schiaua ⁴⁶, R. Schicker ⁹⁵, A. Schmah ⁹⁸, C. Schmidt ⁹⁸, H.R. Schmidt ⁹⁴,
 M.O. Schmidt ³³, M. Schmidt ⁹⁴, N.V. Schmidt ⁸⁸, A.R. Schmier ¹²³, R. Schotter ¹³⁰, A. Schröter ³⁹,
 J. Schukraft ³³, K. Schweda ⁹⁸, G. Scioli ²⁶, E. Scomparin ⁵⁷, J.E. Seger ¹⁵, Y. Sekiguchi ¹²⁵,
 D. Sekihata ¹²⁵, M. Selina ⁸⁵, I. Selyuzhenkov ⁹⁸, S. Senyukov ¹³⁰, J.J. Seo ^{95,59}, D. Serebryakov ¹⁴²,
 L. Šerkšnytė ⁹⁶, A. Sevcenco ⁶⁴, T.J. Shaba ⁶⁹, A. Shabetai ¹⁰⁴, R. Shahoyan ³³, A. Shangaraev ¹⁴²,
 A. Sharma ⁹¹, B. Sharma ⁹², D. Sharma ⁴⁸, H. Sharma ^{55,108}, M. Sharma ⁹², S. Sharma ⁷⁷,
 S. Sharma ⁹², U. Sharma ⁹², A. Shatat ¹³², O. Sheibani ¹¹⁷, K. Shigaki ⁹³, M. Shimomura ⁷⁸, J. Shin ¹²,
 S. Shirinkin ¹⁴², Q. Shou ⁴⁰, Y. Sibiriak ¹⁴², S. Siddhanta ⁵³, T. Siemiarczuk ⁸⁰, T.F. Silva ¹¹¹,
 D. Silvermyr ⁷⁶, T. Simantathammakul ¹⁰⁶, R. Simeonov ³⁷, B. Singh ⁹², B. Singh ⁹⁶, K. Singh ⁴⁹,
 R. Singh ⁸¹, R. Singh ⁹², R. Singh ⁴⁹, S. Singh ¹⁶, V.K. Singh ¹³⁶, V. Singhal ¹³⁶, T. Sinha ¹⁰⁰,
 B. Sitar ¹³, M. Sitta ^{134,57}, T.B. Skaali ²⁰, G. Skorodumovs ⁹⁵, M. Slupecki ⁴⁴, N. Smirnov ¹³⁹,
 R.J.M. Snellings ⁶⁰, E.H. Solheim ²⁰, J. Song ¹¹⁷, A. Songmoolnak ¹⁰⁶, C. Sonnabend ^{33,98},
 F. Soramel ²⁸, A.B. Soto-hernandez ⁸⁹, R. Spijkers ⁸⁵, I. Sputowska ¹⁰⁸, J. Staa ⁷⁶, J. Stachel ⁹⁵,
 I. Stan ⁶⁴, P.J. Steffanic ¹²³, S.F. Stiefelmaier ⁹⁵, D. Stocco ¹⁰⁴, I. Storehaug ²⁰, P. Stratmann ¹²⁷,
 S. Strazzi ²⁶, A. Sturniolo ^{31,54}, C.P. Stylianidis ⁸⁵, A.A.P. Suaide ¹¹¹, C. Suire ¹³², M. Sukhanov ¹⁴²,
 M. Suljic ³³, R. Sultanov ¹⁴², V. Sumberia ⁹², S. Sumowidagdo ⁸³, S. Swain ⁶², I. Szarka ¹³,
 M. Szymkowski ¹³⁷, S.F. Taghavi ⁹⁶, G. Taillepied ⁹⁸, J. Takahashi ¹¹², G.J. Tambave ⁸¹, S. Tang ⁶,
 Z. Tang ¹²¹, J.D. Tapia Takaki ¹¹⁹, N. Tapus ¹¹⁴, L.A. Tarasovicova ¹²⁷, M.G. Tarzila ⁴⁶, G.F. Tassielli ³²,
 A. Tauro ³³, A. Tavira García ¹³², G. Tejeda Muñoz ⁴⁵, A. Telesca ³³, L. Terlizzi ²⁵, C. Terrevoli ¹¹⁷,
 S. Thakur ⁴, D. Thomas ¹⁰⁹, F. Thoresen ⁸⁴, A. Tikhonov ¹⁴², A.R. Timmins ¹¹⁷, M. Tkacik ¹⁰⁷,
 T. Tkacik ¹⁰⁷, A. Toia ⁶⁵, R. Tokumoto ⁹³, K. Tomohiro ⁹³, N. Topilskaya ¹⁴², M. Toppi ⁵⁰, T. Tork ¹³²,
 V.V. Torres ¹⁰⁴, A.G. Torres Ramos ³², A. Trifiró ^{31,54}, A.S. Triolo ^{33,31,54}, S. Tripathy ⁵²,
 T. Tripathy ⁴⁸, S. Trogolo ³³, V. Trubnikov ³, W.H. Trzaska ¹¹⁸, T.P. Trzcinski ¹³⁷, A. Tumkin ¹⁴²,
 R. Turrisi ⁵⁵, T.S. Tveter ²⁰, K. Ullaland ²¹, B. Ulukutlu ⁹⁶, A. Uras ¹²⁹, G.L. Usai ²³, M. Vala ³⁸,
 N. Valle ²², L.V.R. van Doremalen ⁶⁰, M. van Leeuwen ⁸⁵, C.A. van Veen ⁹⁵, R.J.G. van Weelden ⁸⁵,
 P. Vande Vyvre ³³, D. Varga ⁴⁷, Z. Varga ⁴⁷, M. Vasileiou ⁷⁹, A. Vasiliev ¹⁴², O. Vázquez Doce ⁵⁰,
 O. Vazquez Rueda ¹¹⁷, V. Vechernin ¹⁴², E. Vercellin ²⁵, S. Vergara Limón ⁴⁵, R. Verma ⁴⁸, L. Vermunt ⁹⁸,
 R. Vértesi ⁴⁷, M. Verweij ⁶⁰, L. Vickovic ³⁴, Z. Vilakazi ¹²⁴, O. Villalobos Baillie ¹⁰¹, A. Villani ²⁴,
 G. Vino ⁵¹, A. Vinogradov ¹⁴², T. Virgili ²⁹, M.M.O. Virta ¹¹⁸, V. Vislavicius ⁷⁶, A. Vodopyanov ¹⁴³,
 B. Volkel ³³, M.A. Völk ⁹⁵, K. Voloshin ¹⁴², S.A. Voloshin ¹³⁸, G. Volpe ³², B. von Haller ³³,
 I. Vorobyev ⁹⁶, N. Vozniuk ¹⁴², J. Vrláková ³⁸, J. Wan ⁴⁰, C. Wang ⁴⁰, D. Wang ⁴⁰, Y. Wang ⁴⁰,
 Y. Wang ⁶, A. Wegrzynek ³³, F.T. Weighofer ³⁹, S.C. Wenzel ³³, J.P. Wessels ¹²⁷, J. Wiechula ⁶⁵,
 J. Wikne ²⁰, G. Wilk ⁸⁰, J. Wilkinson ⁹⁸, G.A. Willems ¹²⁷, B. Windelband ⁹⁵, M. Winn ¹³¹,

J.R. Wright ¹⁰⁹, W. Wu⁴⁰, Y. Wu ¹²¹, R. Xu ⁶, A. Yadav ⁴³, A.K. Yadav ¹³⁶, S. Yalcin ⁷³, Y. Yamaguchi ⁹³, S. Yang²¹, S. Yano ⁹³, Z. Yin ⁶, I.-K. Yoo ¹⁷, J.H. Yoon ⁵⁹, H. Yu¹², S. Yuan²¹, A. Yuncu ⁹⁵, V. Zaccolo ²⁴, C. Zampolli ³³, F. Zanone ⁹⁵, N. Zardoshti ³³, A. Zarochentsev ¹⁴², P. Závada ⁶³, N. Zaviyalov¹⁴², M. Zhalov ¹⁴², B. Zhang ⁶, C. Zhang ¹³¹, L. Zhang ⁴⁰, S. Zhang ⁴⁰, X. Zhang ⁶, Y. Zhang¹²¹, Z. Zhang ⁶, M. Zhao ¹⁰, V. Zherebchevskii ¹⁴², Y. Zhi¹⁰, D. Zhou ⁶, Y. Zhou ⁸⁴, J. Zhu ^{55,6}, Y. Zhu⁶, S.C. Zugravel ⁵⁷, N. Zurlo ^{135,56}

Affiliation Notes

^I Deceased

^{II} Also at: Max-Planck-Institut fur Physik, Munich, Germany

^{III} Also at: Italian National Agency for New Technologies, Energy and Sustainable Economic Development (ENEA), Bologna, Italy

^{IV} Also at: Dipartimento DET del Politecnico di Torino, Turin, Italy

^V Also at: Department of Applied Physics, Aligarh Muslim University, Aligarh, India

^{VI} Also at: Institute of Theoretical Physics, University of Wroclaw, Poland

^{VII} Also at: An institution covered by a cooperation agreement with CERN

Collaboration Institutes

¹ A.I. Alikhanyan National Science Laboratory (Yerevan Physics Institute) Foundation, Yerevan, Armenia

² AGH University of Krakow, Cracow, Poland

³ Bogolyubov Institute for Theoretical Physics, National Academy of Sciences of Ukraine, Kiev, Ukraine

⁴ Bose Institute, Department of Physics and Centre for Astroparticle Physics and Space Science (CAPSS), Kolkata, India

⁵ California Polytechnic State University, San Luis Obispo, California, United States

⁶ Central China Normal University, Wuhan, China

⁷ Centro de Aplicaciones Tecnológicas y Desarrollo Nuclear (CEADEN), Havana, Cuba

⁸ Centro de Investigación y de Estudios Avanzados (CINVESTAV), Mexico City and Mérida, Mexico

⁹ Chicago State University, Chicago, Illinois, United States

¹⁰ China Institute of Atomic Energy, Beijing, China

¹¹ China University of Geosciences, Wuhan, China

¹² Chungbuk National University, Cheongju, Republic of Korea

¹³ Comenius University Bratislava, Faculty of Mathematics, Physics and Informatics, Bratislava, Slovak Republic

¹⁴ COMSATS University Islamabad, Islamabad, Pakistan

¹⁵ Creighton University, Omaha, Nebraska, United States

¹⁶ Department of Physics, Aligarh Muslim University, Aligarh, India

¹⁷ Department of Physics, Pusan National University, Pusan, Republic of Korea

¹⁸ Department of Physics, Sejong University, Seoul, Republic of Korea

¹⁹ Department of Physics, University of California, Berkeley, California, United States

²⁰ Department of Physics, University of Oslo, Oslo, Norway

²¹ Department of Physics and Technology, University of Bergen, Bergen, Norway

²² Dipartimento di Fisica, Università di Pavia, Pavia, Italy

²³ Dipartimento di Fisica dell'Università and Sezione INFN, Cagliari, Italy

²⁴ Dipartimento di Fisica dell'Università and Sezione INFN, Trieste, Italy

²⁵ Dipartimento di Fisica dell'Università and Sezione INFN, Turin, Italy

²⁶ Dipartimento di Fisica e Astronomia dell'Università and Sezione INFN, Bologna, Italy

²⁷ Dipartimento di Fisica e Astronomia dell'Università and Sezione INFN, Catania, Italy

²⁸ Dipartimento di Fisica e Astronomia dell'Università and Sezione INFN, Padova, Italy

²⁹ Dipartimento di Fisica 'E.R. Caianiello' dell'Università and Gruppo Collegato INFN, Salerno, Italy

³⁰ Dipartimento DISAT del Politecnico and Sezione INFN, Turin, Italy

³¹ Dipartimento di Scienze MIFT, Università di Messina, Messina, Italy

³² Dipartimento Interateneo di Fisica 'M. Merlin' and Sezione INFN, Bari, Italy

³³ European Organization for Nuclear Research (CERN), Geneva, Switzerland

³⁴ Faculty of Electrical Engineering, Mechanical Engineering and Naval Architecture, University of Split, Split, Croatia

- ³⁵ Faculty of Engineering and Science, Western Norway University of Applied Sciences, Bergen, Norway
³⁶ Faculty of Nuclear Sciences and Physical Engineering, Czech Technical University in Prague, Prague, Czech Republic
³⁷ Faculty of Physics, Sofia University, Sofia, Bulgaria
³⁸ Faculty of Science, P.J. Šafárik University, Košice, Slovak Republic
³⁹ Frankfurt Institute for Advanced Studies, Johann Wolfgang Goethe-Universität Frankfurt, Frankfurt, Germany
⁴⁰ Fudan University, Shanghai, China
⁴¹ Gangneung-Wonju National University, Gangneung, Republic of Korea
⁴² Gauhati University, Department of Physics, Guwahati, India
⁴³ Helmholtz-Institut für Strahlen- und Kernphysik, Rheinische Friedrich-Wilhelms-Universität Bonn, Bonn, Germany
⁴⁴ Helsinki Institute of Physics (HIP), Helsinki, Finland
⁴⁵ High Energy Physics Group, Universidad Autónoma de Puebla, Puebla, Mexico
⁴⁶ Horia Hulubei National Institute of Physics and Nuclear Engineering, Bucharest, Romania
⁴⁷ HUN-REN Wigner Research Centre for Physics, Budapest, Hungary
⁴⁸ Indian Institute of Technology Bombay (IIT), Mumbai, India
⁴⁹ Indian Institute of Technology Indore, Indore, India
⁵⁰ INFN, Laboratori Nazionali di Frascati, Frascati, Italy
⁵¹ INFN, Sezione di Bari, Bari, Italy
⁵² INFN, Sezione di Bologna, Bologna, Italy
⁵³ INFN, Sezione di Cagliari, Cagliari, Italy
⁵⁴ INFN, Sezione di Catania, Catania, Italy
⁵⁵ INFN, Sezione di Padova, Padova, Italy
⁵⁶ INFN, Sezione di Pavia, Pavia, Italy
⁵⁷ INFN, Sezione di Torino, Turin, Italy
⁵⁸ INFN, Sezione di Trieste, Trieste, Italy
⁵⁹ Inha University, Incheon, Republic of Korea
⁶⁰ Institute for Gravitational and Subatomic Physics (GRASP), Utrecht University/Nikhef, Utrecht, Netherlands
⁶¹ Institute of Experimental Physics, Slovak Academy of Sciences, Košice, Slovak Republic
⁶² Institute of Physics, Homi Bhabha National Institute, Bhubaneswar, India
⁶³ Institute of Physics of the Czech Academy of Sciences, Prague, Czech Republic
⁶⁴ Institute of Space Science (ISS), Bucharest, Romania
⁶⁵ Institut für Kernphysik, Johann Wolfgang Goethe-Universität Frankfurt, Frankfurt, Germany
⁶⁶ Instituto de Ciencias Nucleares, Universidad Nacional Autónoma de México, Mexico City, Mexico
⁶⁷ Instituto de Física, Universidade Federal do Rio Grande do Sul (UFRGS), Porto Alegre, Brazil
⁶⁸ Instituto de Física, Universidad Nacional Autónoma de México, Mexico City, Mexico
⁶⁹ iThemba LABS, National Research Foundation, Somerset West, South Africa
⁷⁰ Jeonbuk National University, Jeonju, Republic of Korea
⁷¹ Johann-Wolfgang-Goethe Universität Frankfurt Institut für Informatik, Fachbereich Informatik und Mathematik, Frankfurt, Germany
⁷² Korea Institute of Science and Technology Information, Daejeon, Republic of Korea
⁷³ KTO Karatay University, Konya, Turkey
⁷⁴ Laboratoire de Physique Subatomique et de Cosmologie, Université Grenoble-Alpes, CNRS-IN2P3, Grenoble, France
⁷⁵ Lawrence Berkeley National Laboratory, Berkeley, California, United States
⁷⁶ Lund University Department of Physics, Division of Particle Physics, Lund, Sweden
⁷⁷ Nagasaki Institute of Applied Science, Nagasaki, Japan
⁷⁸ Nara Women's University (NWU), Nara, Japan
⁷⁹ National and Kapodistrian University of Athens, School of Science, Department of Physics , Athens, Greece
⁸⁰ National Centre for Nuclear Research, Warsaw, Poland
⁸¹ National Institute of Science Education and Research, Homi Bhabha National Institute, Jatni, India
⁸² National Nuclear Research Center, Baku, Azerbaijan
⁸³ National Research and Innovation Agency - BRIN, Jakarta, Indonesia
⁸⁴ Niels Bohr Institute, University of Copenhagen, Copenhagen, Denmark
⁸⁵ Nikhef, National institute for subatomic physics, Amsterdam, Netherlands
⁸⁶ Nuclear Physics Group, STFC Daresbury Laboratory, Daresbury, United Kingdom

- ⁸⁷ Nuclear Physics Institute of the Czech Academy of Sciences, Husinec-Řež, Czech Republic
⁸⁸ Oak Ridge National Laboratory, Oak Ridge, Tennessee, United States
⁸⁹ Ohio State University, Columbus, Ohio, United States
⁹⁰ Physics department, Faculty of science, University of Zagreb, Zagreb, Croatia
⁹¹ Physics Department, Panjab University, Chandigarh, India
⁹² Physics Department, University of Jammu, Jammu, India
⁹³ Physics Program and International Institute for Sustainability with Knotted Chiral Meta Matter (SKCM2), Hiroshima University, Hiroshima, Japan
⁹⁴ Physikalischs Institut, Eberhard-Karls-Universität Tübingen, Tübingen, Germany
⁹⁵ Physikalischs Institut, Ruprecht-Karls-Universität Heidelberg, Heidelberg, Germany
⁹⁶ Physik Department, Technische Universität München, Munich, Germany
⁹⁷ Politecnico di Bari and Sezione INFN, Bari, Italy
⁹⁸ Research Division and ExtreMe Matter Institute EMMI, GSI Helmholtzzentrum für Schwerionenforschung GmbH, Darmstadt, Germany
⁹⁹ Saga University, Saga, Japan
¹⁰⁰ Saha Institute of Nuclear Physics, Homi Bhabha National Institute, Kolkata, India
¹⁰¹ School of Physics and Astronomy, University of Birmingham, Birmingham, United Kingdom
¹⁰² Sección Física, Departamento de Ciencias, Pontificia Universidad Católica del Perú, Lima, Peru
¹⁰³ Stefan Meyer Institut für Subatomare Physik (SMI), Vienna, Austria
¹⁰⁴ SUBATECH, IMT Atlantique, Nantes Université, CNRS-IN2P3, Nantes, France
¹⁰⁵ Sungkyunkwan University, Suwon City, Republic of Korea
¹⁰⁶ Suranaree University of Technology, Nakhon Ratchasima, Thailand
¹⁰⁷ Technical University of Košice, Košice, Slovak Republic
¹⁰⁸ The Henryk Niewodniczanski Institute of Nuclear Physics, Polish Academy of Sciences, Cracow, Poland
¹⁰⁹ The University of Texas at Austin, Austin, Texas, United States
¹¹⁰ Universidad Autónoma de Sinaloa, Culiacán, Mexico
¹¹¹ Universidade de São Paulo (USP), São Paulo, Brazil
¹¹² Universidade Estadual de Campinas (UNICAMP), Campinas, Brazil
¹¹³ Universidade Federal do ABC, Santo Andre, Brazil
¹¹⁴ Universitatea Națională de Știință și Tehnologie Politehnica Bucuresti, Bucharest, Romania
¹¹⁵ University of Cape Town, Cape Town, South Africa
¹¹⁶ University of Derby, Derby, United Kingdom
¹¹⁷ University of Houston, Houston, Texas, United States
¹¹⁸ University of Jyväskylä, Jyväskylä, Finland
¹¹⁹ University of Kansas, Lawrence, Kansas, United States
¹²⁰ University of Liverpool, Liverpool, United Kingdom
¹²¹ University of Science and Technology of China, Hefei, China
¹²² University of South-Eastern Norway, Kongsberg, Norway
¹²³ University of Tennessee, Knoxville, Tennessee, United States
¹²⁴ University of the Witwatersrand, Johannesburg, South Africa
¹²⁵ University of Tokyo, Tokyo, Japan
¹²⁶ University of Tsukuba, Tsukuba, Japan
¹²⁷ Universität Münster, Institut für Kernphysik, Münster, Germany
¹²⁸ Université Clermont Auvergne, CNRS/IN2P3, LPC, Clermont-Ferrand, France
¹²⁹ Université de Lyon, CNRS/IN2P3, Institut de Physique des 2 Infinis de Lyon, Lyon, France
¹³⁰ Université de Strasbourg, CNRS, IPHC UMR 7178, F-67000 Strasbourg, France, Strasbourg, France
¹³¹ Université Paris-Saclay, Centre d'Etudes de Saclay (CEA), IRFU, Département de Physique Nucléaire (DPhN), Saclay, France
¹³² Université Paris-Saclay, CNRS/IN2P3, IJCLab, Orsay, France
¹³³ Università degli Studi di Foggia, Foggia, Italy
¹³⁴ Università del Piemonte Orientale, Vercelli, Italy
¹³⁵ Università di Brescia, Brescia, Italy
¹³⁶ Variable Energy Cyclotron Centre, Homi Bhabha National Institute, Kolkata, India
¹³⁷ Warsaw University of Technology, Warsaw, Poland
¹³⁸ Wayne State University, Detroit, Michigan, United States
¹³⁹ Yale University, New Haven, Connecticut, United States

¹⁴⁰ Yonsei University, Seoul, Republic of Korea

¹⁴¹ Zentrum für Technologie und Transfer (ZTT), Worms, Germany

¹⁴² Affiliated with an institute covered by a cooperation agreement with CERN

¹⁴³ Affiliated with an international laboratory covered by a cooperation agreement with CERN.